SCATTERING BY A SEMI-INFINITE LATTICE AND THE EXCITATION OF BLOCH WAVES

by N. TYMIS

(*Archimedes Center for Modeling, Analysis & Computation Department of Applied Mathematics, Students' Center Building, Voutes Campus, University of Crete P.O. Box 2208, 71003 Heraklion, Crete, Greece*)

I. THOMPSON

(*Department of Mathematical Sciences, University of Liverpool, Liverpool L69 7ZL, UK*)

[Submitted 24 October 2013]

Summary

The interaction of a time-harmonic plane wave with a semi-infinite lattice of identical circular cylinders is considered, using a formulation that allows for cylinders of finite size that do not scatter isotropically. Multipole expansions and Graf's addition theorem are used to reduce the boundary value problem to an infinite linear system of equations. Applying the z transform and disregarding interaction effects due to certain strongly damped modes then leads to a matrix Wiener–Hopf equation with rational elements. This is solved by a straightforward method that does not require matrix factorisation. Implementation of the method requires that the zeros of the matrix determinant be located numerically, and once this is achieved, all far field quantities can be calculated. Numerical results that show the proportion of energy reflected back from the edge are presented for several different lattice geometries.

1. Introduction

Bloch waves can propagate through periodic media without loss of energy, and have been found to exist in a range of different physical contexts, including elastodynamics of composite materials and thin plates, acoustics and electromagnetism (**1**, **2**, **3**, **4**). Bloch wave propagation continues to be an active research field; recent papers that have introduced new ideas include (**5**, **6**) and (**7**). Associated with each periodic medium that supports Bloch waves is a band structure that dictates the parameter regimes where propagation is permitted. A given frequency may lie in a total stop band where no propagation is possible, a partial stop band where propagation can occur in a limited set of directions, or a pass band where propagation in any direction is possible. This complex, frequency and direction dependent behaviour leads to important applications in the fabrication of waveguides, filters, optical fibres and photonic crystals (**8**, **9**, **10**). The band structure can be used to make some deductions about the scattered field that arises when an incident wave strikes the edge of a periodic medium. If the parameters lie in a stop band then no transmission is possible, and all of the incident wave energy must be reflected back from the edge. If transmission is possible, some or all of the incident energy may be converted into Bloch waves, but it is not possible to make a quantitative statement about the amplitudes of the transmitted and reflected fields based on the band structure alone (**10**, pp. 223–224). This

excitation problem has received far less attention than the propagation problems discussed above, but some papers on the subject have appeared in the last few years. In (**11**), the present authors considered scattering of a plane acoustic wave by a semi-infinite periodic medium. This work was carried out under the assumption that the scattering from each lattice element is isotropic, which is only valid if the surfaces of the scatterers are sound-soft, and the wavelength is large in comparison to the other length scales in the problem. Electromagnetic scattering by a three-dimensional lattice has been considered in (**12**) using a single point dipole approximation to represent nanospheres making up the lattice. Some general characteristics of problems involving larger lattice elements are considered in (**13**), but explicit solutions are only given for point dipoles.

In this paper, we develop a method that can be applied to problems where finite size effects are important, so that the scatterers cannot be modelled as points. Our analysis allows for lattice elements that do not scatter isotropically, and remains applicable when the wavelength is comparable to the scatterer size. The key improvement is the use of multipole expansions to represent the scattered field. We will consider the canonical problem of an acoustic plane wave incident on a semi-infinite lattice (a semi-infinite stack of infinite rows) of identical circular cylinders. We assume there is no variation along the axis of the cylinders, so that the problem is governed by the two-dimensional Helmholtz equation. The low frequency limit considered in (**11**) is a special case of this analysis, and can be retrieved by discarding all but one of the terms (the monopole) from each multipole expansion. Since the focus of this article is on the development of our method, we choose to avoid the introduction of additional parameters where possible. Consequently, in what follows, we will consider only sound-soft and sound-hard boundary conditions, so that there is no field inside the cylinders. These boundary conditions can occur in other physical contexts. In electromagnetism, transverse magnetic and transverse electric waves incident on a semi-infinite lattice of perfectly conducting cylinders lead to problems equivalent to the sound-soft and sound-hard cases, respectively (**14**, pp. 13, 19). In linear water wave theory, a plane wave incident on a semi-infinite lattice of bottom-mounted, surface penetrating cylinders is equivalent to the sound-hard case (**15**, ch. 2). For completeness, we note that other boundary conditions can be applied by changing the scattering coefficients (denoted by Z_n in our subsequent analysis) used to relate the fields incoming toward and outgoing from each lattice element. The scattering coefficients that we use are special cases of a more general coefficient that accounts for penetrable cylinders; see (**16**, Section IV A) for details.

The plan of the paper is as follows. In Section 2 we formulate the boundary value problem, and in Sections 3–4 we derive representations of the field in terms of grating modes and multipole expansions. Applying Graf's addition theorem (**14**, Theorem 2.12) to the multipole representation leads to an infinite linear system of equations. When Bloch waves are excited, this system has poor convergence properties, and cannot be solved directly by truncation, but it is amenable to the discrete Wiener–Hopf technique (**17**, **18**). Following the method of (**11**), in Section 5 we apply the z transform (**19**) to obtain a Wiener–Hopf equation. A key difference between the low frequency analysis in our earlier article and the current work then becomes apparent. The Wiener–Hopf equation obtained in (**11**) is scalar, that is it consists of a single functional equation containing two unknown functions, which have known (and overlapping) domains of analyticity. Equations of this type can be solved using a standard procedure (**20**, Section 1.7). For the current problem, we obtain an infinite-dimensional matrix Wiener–Hopf equation (an infinite set of coupled scalar equations). This turns

out to have some important symmetry properties, and these are the subject of Section 6. In Section 7, we truncate the multipole expansions to obtain a finite-dimensional matrix Wiener–Hopf equation. Then, by neglecting interaction effects due to strongly evanescent grating modes, we further reduce this to an equation whose elements are rational functions. This approximate system is solved by matching the poles and residues on opposing sides, and in this way we avoid the necessity of performing a matrix Wiener–Hopf factorisation, which is generally very difficult (**21**, **22**). After solving the Wiener–Hopf equation, we proceed to analyse the transmitted and reflected far field patterns in Section 8. Using these, we derive a conservation of energy condition in Section 9, which is used as a check on our numerical results, and to ensure that no Bloch waves that transport energy toward the interface are included in our solutions. Some details of the implementation are given in Section 10, and numerical results are presented with discussion in Section 11. Finally, some concluding remarks are made in Section 12.

2. Formulation

Let $\mathbf{a}_1$ and $\mathbf{a}_2$ be linearly independent vectors in the (x, y) plane. Suppose that infinitely long (in z), cylindrical scatterers of radius ℓ are centred at the points with position vectors

$$\mathbf{R}_{jp} = j\mathbf{a}_1 + p\mathbf{a}_2, \quad j \in \mathbb{Z}, \quad p = 0, 1, \ldots \tag{2.1}$$

forming a semi-infinite lattice (Fig. 1). Without loss of generality, we can assume that

$$\mathbf{a}_1 = a_1\hat{\mathbf{x}}, \quad \text{and} \quad \mathbf{a}_2 = \eta_1\hat{\mathbf{x}} + \eta_2\hat{\mathbf{y}}, \tag{2.2}$$

where $\eta_2 > 0$. Here, $\hat{\mathbf{x}}$ and $\hat{\mathbf{y}}$ are unit vectors in the x and y directions, respectively, and we have introduced the convention that $|\mathbf{v}| = v$ for any vector $\mathbf{v}$, which will be used throughout. In order that the cylinders do not overlap, we must have $a > 2\ell$, where a is the magnitude of the shortest nonzero lattice vector, that is

$$a = \min_{j^2+p^2\neq 0} R_{jp}. \tag{2.3}$$

We also introduce position vectors relative to the centre of each cylinder; thus

$$\mathbf{r}_{jp} = \mathbf{r} - \mathbf{R}_{jp}, \tag{2.4}$$

as shown in Fig. 1. We will consider time-harmonic motion with frequency ω, in which case the acoustic potential outside the cylinders is given by

$$U(\mathbf{r}, t) = \operatorname{Re}\left[u(\mathbf{r})e^{-i\omega t}\right]. \tag{2.5}$$

The complex-valued function u must satisfy the Helmholtz equation

$$\left(\nabla^2 + k^2\right)u(\mathbf{r}) = 0, \tag{2.6}$$

where $k = \omega/c$, with c representing the speed of sound. For sound-soft cylinders, the surfaces are subject to the Dirichlet boundary condition

$$u(\mathbf{r}) = 0 \quad \text{on} \quad r_{jp} = \ell, \quad j \in \mathbb{Z}, \quad p = 0, 1, \ldots \tag{2.7}$$

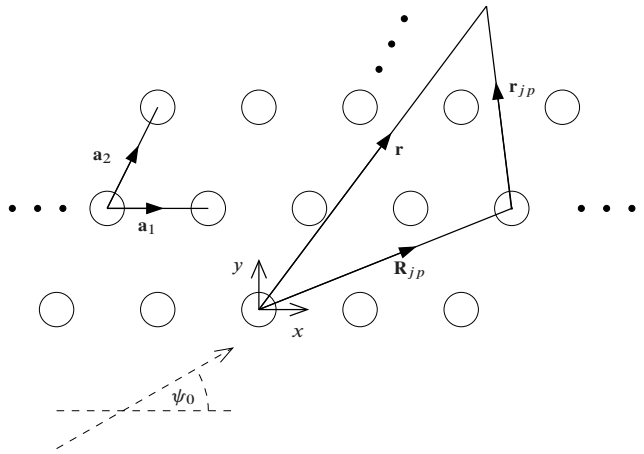

Fig. 1 Schematic diagram showing a section of the lattice, and illustrating the notation in use.

whereas for sound-hard cylinders the Neumann condition

$$\frac{\partial u(\mathbf{r})}{\partial r_{jp}} = 0 \quad \text{on} \quad r_{jp} = \ell, \quad j \in \mathbb{Z}, \quad p = 0, 1, \ldots \tag{2.8}$$

applies. Let the plane wave corresponding to

$$u^{\mathrm{i}}(\mathbf{r}) = e^{i\mathbf{r}\cdot\mathbf{k}} \tag{2.9}$$

be incident upon the lattice, where the wavenumber vector is given by

$$\mathbf{k} = k\cos\psi_0\,\hat{\mathbf{x}} + k\sin\psi_0\,\hat{\mathbf{y}}, \quad \psi_0 \in (0, \pi). \tag{2.10}$$

The total field is then given by

$$u = u^{\mathrm{i}} + u^{\mathrm{s}}, \tag{2.11}$$

where u^{s} is the scattered field, which we seek to determine. In order to match the periodicity of the geometry and of the incident field we must have

$$u(\mathbf{r} + j\mathbf{a}_1) = e^{ijka_1\cos\psi_0}u(\mathbf{r}), \quad j \in \mathbb{Z}, \tag{2.12}$$

and the same condition applies to the scattered field.

3. Grating mode representation

At points that do not lies on the axes of the rows, so that there is no nonnegative integer q such that $y = q\eta_2$, the scattered field can be represented as a sum of grating modes, each of which is an exponential solution to the Helmholtz equation that satisfies the quasi-periodicity condition (2.12). That is,

$$u(\mathbf{r}) = \sum_{j=-\infty}^{\infty} e^{ikx\cos\psi_j}\left[c_j^+ e^{iky\sin\psi_j} + c_j^- e^{-iky\sin\psi_j}\right], \tag{3.1}$$

for some unknown amplitude coefficients $c_j^{\pm}$. Here, the scattering angles are defined via

$$k\cos\psi_j = k\cos\psi_0 + 2j\pi/a_1, \quad \text{and} \quad k\sin\psi_j = i\gamma(k\cos\psi_j), \tag{3.2}$$

where the function γ is given by

$$\gamma(t) = \begin{cases} \sqrt{t^2-k^2} & \text{if } |t| \geq k, \\ -i\sqrt{k^2-t^2} & \text{if } |t| < k. \end{cases} \tag{3.3}$$

Note that $\cos\psi_j$ is always real, whereas $\sin\psi_j$ is positive real for a finite set of integers j and positive imaginary otherwise. Since the distinction between these two cases is important, we define the sets

$$\mathcal{M} = \{j \in \mathbb{Z} : \ |\cos\psi_j| \leq 1\} \quad \text{and} \quad \mathcal{N} = \{j \in \mathbb{Z} : \ |\cos\psi_j| > 1\}. \tag{3.4}$$

For each $j \in \mathcal{M}$, the grating modes with amplitude coefficients c_j^+ and c_j^- propagate in the direction of increasing and decreasing y, respectively, unless $\sin\psi_j = 0$, in which case they are independent of y. Similarly, for $j \in \mathcal{N}$, modes with amplitude coefficients c_j^+ decay exponentially as y is increased, and those with amplitude coefficients c_j^- decay exponentially as y is decreased. For the problem under consideration here, we should expect the amplitude coefficients to take different values between each pair of rows. An expansion of the form (3.1) also holds in the half-space $y < 0$, but here the scattered field clearly cannot include any modes that grow with decreasing y, or are incoming from infinity. Hence,

$$u^{\mathrm{s}}(\mathbf{r}) = \sum_{j=-\infty}^{\infty} e^{ikx\cos\psi_j}\left[c_{jq}^+ e^{iky\sin\psi_j} + c_{jq}^- e^{-iky\sin\psi_j}\right], \quad (q-1) < \frac{y}{\eta_2} < q, \quad q \in \mathbb{N}, \tag{3.5}$$

and

$$u^{\mathrm{s}}(\mathbf{r}) = \sum_{j=-\infty}^{\infty} c_{j0}^- e^{ik(x\cos\psi_j - y\sin\psi_j)}, \quad y < 0. \tag{3.6}$$

Values for c_{j0}^- and for $c_{jq}^{\pm}$ in the far field limit $q \to \infty$ will be determined in Sections 8 and 9, respectively.

4. Multipole representation

In view of the quasi-periodicity condition (2.12), the multipole expansion (**14**, Chapter 4) for the scattered field has the form

$$u^{\mathrm{s}}(\mathbf{r}) = \sum_{n=-\infty}^{\infty}\sum_{p=0}^{\infty}\sum_{j=-\infty}^{\infty} A_n^p e^{ijka_1\cos\psi_0}\mathcal{H}_n(\mathbf{r}_{jp}). \tag{4.1}$$

Here, the outgoing wavefunction in the summand is defined as

$$\mathcal{H}_n(\mathbf{r}) = H_n^{(1)}(kr)e^{in\theta}, \tag{4.2}$$

where $H_n^{(1)}$ is a Hankel function of the first kind and θ is the anticlockwise angle between the positive x axis and the vector $\mathbf{r}$. Note the symmetry property

$$\mathcal{H}_n(-\mathbf{r}) = (-1)^n\mathcal{H}_n(\mathbf{r}). \tag{4.3}$$

The expansion (4.1) satisfies the Helmholtz equation (2.6), and the amplitude coefficients A_n^p must be chosen so that the boundary condition on the cylinder surfaces is satisfied. The first step in determining the appropriate values for A_n^p is to locally expand the total field about one of the cylinder centres. We need only account for the boundary conditions on cylinders centred at $\mathbf{r} = q\mathbf{a}_2$ for $q = 0, 1, \ldots$ Conditions elsewhere follow automatically, in view of the quasi-periodicity property (2.12). For the incident wave, we use the generating function for Bessel functions (**23**, Equation 10.12.1) and the fact that $u^{\mathrm{i}}(\mathbf{r}) = u^{\mathrm{i}}(\mathbf{R}_{jp})u^{\mathrm{i}}(\mathbf{r}_{jp})$ to obtain the Jacobi expansion

$$u^{\mathrm{i}}(\mathbf{r}) = e^{iq\mathbf{a}_2\cdot\mathbf{k}} \sum_{n=-\infty}^{\infty} i^n e^{-in\psi_0} \mathcal{J}_n(\mathbf{r}_{0q}), \tag{4.4}$$

where the regular wavefunction $\mathcal{J}_n(\cdot)$ is given by

$$\mathcal{J}_n(\mathbf{r}) = J_n(kr)e^{in\theta}, \tag{4.5}$$

with θ defined as in equation (4.2). For the scattered field, we use Graf's addition theorem (**14**, Theorem 2.12), which in our notation shows that

$$\mathcal{H}_n(\mathbf{r}_{jp}) = \sum_{m=-\infty}^{\infty} \mathcal{H}_{n-m}(-\mathbf{R}_{j,p-q})\mathcal{J}_m(\mathbf{r}_{0q}), \quad n \in \mathbb{Z}, \quad r_{0q} < R_{j,p-q}. \tag{4.6}$$

Terms in the multipole expansion (4.1) with $j = 0$ and $p = q$ represent the field radiating from the cylinder centred at $\mathbf{r} = q\mathbf{a}_2$, and do not need to be re-expanded. Using (4.6) for the remainder of the series, we obtain

$$u^{\mathrm{s}}(\mathbf{r}) = \sum_{n=-\infty}^{\infty} \left[A_n^q \mathcal{H}_n(\mathbf{r}_{0q}) + \sum_{p=0}^{\infty} {\sum_{j=-\infty}^{\infty}}' A_n^p e^{ijka_1\cos\psi_0} \sum_{m=-\infty}^{\infty} \mathcal{H}_{n-m}(-\mathbf{R}_{j,p-q})\mathcal{J}_m(\mathbf{r}_{0q}) \right], \tag{4.7}$$

where the prime symbol indicates that the terms in which $R_{j,p-q} = 0$ are to be omitted from the summation. This expansion is valid provided that $r_{0q} < a$, where a is given by (2.3). Combining (4.7) with (4.4) yields the local expansion

$$u(\mathbf{r}) = \sum_{n=-\infty}^{\infty} \left[A_n^q \mathcal{H}_n(\mathbf{r}_{0q}) + I_n^q \mathcal{J}_n(\mathbf{r}_{0q}) \right], \quad r_{0q} < a, \quad q = 0, 1, \ldots \tag{4.8}$$

Here, the second term on the right-hand side represents the field incident on the cylinder centred at $r_{0q} = 0$, consisting of the incident plane wave, and the radiation from all the other cylinders. An expression for I_n^q can be obtained by reading off the coefficient of the regular wavefunction in (4.7) and combining this with the contribution from (4.4). In this way, we find that

$$I_n^q = i^n e^{i(q\mathbf{a}_2\cdot\mathbf{k} - n\psi_0)} + \sum_{m=-\infty}^{\infty} \sum_{p=0}^{\infty} {\sum_{j=-\infty}^{\infty}}' A_m^p e^{ijka_1\cos\psi_0} \mathcal{H}_{m-n}(-\mathbf{R}_{j,p-q}). \tag{4.9}$$

After separating the term in which $p = q$, we rewrite this in the form

$$I_n^q = i^n e^{i(q\mathbf{a}_2\cdot\mathbf{k}-n\psi_0)} + \sum_{m=-\infty}^{\infty}\sum_{p=0}^{\infty} A_m^p S_{m-n}^{q-p}(k\cos\psi_0), \quad n\in\mathbb{Z}, \quad q = 0,1,\dots \tag{4.10}$$

where

$$S_n^q(k\cos\psi_0) = \begin{cases} \sigma_{-n}(k\cos\psi_0) & \text{if } q = 0, \\ G_n(q\mathbf{a}_2, k\cos\psi_0) & \text{if } q \neq 0. \end{cases} \tag{4.11}$$

Here, the quasi-periodic Green's function G_n and the lattice sum σ_n are defined via

$$G_n(\mathbf{r},\beta_x) = \sum_{j=-\infty}^{\infty} e^{ija_1\beta_x}\mathcal{H}_n(\mathbf{r}-\mathbf{R}_{j0}) \tag{4.12}$$

and

$$\sigma_n(\beta_x) = \sum_{\substack{j=-\infty \\ j\neq 0}}^{\infty} e^{ija_1\beta_x}\mathcal{H}_n(j\mathbf{a}_1). \tag{4.13}$$

Further details of these functions are given in appendices A and B, respectively. Applying the boundary condition on $r_{0q} = \ell$ and using the orthogonality of the cylindrical harmonics in the wavefunctions $\mathcal{H}_n$ and $\mathcal{J}_n$ in (4.8), we find that

$$A_n^q + Z_n I_n^q = 0, \tag{4.14}$$

where the scattering coefficient Z_n is given by

$$Z_n = J_n(k\ell)\big/H_n^{(1)}(k\ell) \tag{4.15}$$

for Dirichlet conditions, whereas for Neumann conditions we have

$$Z_n = J_n'(k\ell)\big/H_n^{(1)\prime}(k\ell). \tag{4.16}$$

Eliminating I_n^q from (4.14) using (4.10) leads to the system of equations

$$A_n^q + Z_n\sum_{m=-\infty}^{\infty}\sum_{p=0}^{\infty} A_m^p S_{m-n}^{q-p}(k\cos\psi_0) = -Z_n i^n e^{i(q\mathbf{a}_2\cdot\mathbf{k}-n\psi_0)}, \quad n\in\mathbb{Z}, \quad q = 0,1,\dots \tag{4.17}$$

The magnitude of Z_n decays rapidly as $|n|\to\infty$, due to the asymptotic behaviour of the Bessel and Hankel functions in this limit (**23**, Section 10.19). On the other hand, when Bloch waves are excited, $A_m^p \not\to 0$ as $p\to\infty$. Therefore (4.17) cannot be solved by truncation, and we must treat the sum over p analytically. Before doing so, we note that for both types of boundary condition under consideration (and also for penetrable cylinders, see (**24**) — this paper contains the equivalent calculation for spherical wavefunctions, but the algebra for the two-dimensional case is the same) the coefficients Z_n have the important property that

$$Z_n/(1-Z_n) = -i\,W_n, \tag{4.18}$$

where W_n is real. It turns out to be advantageous to work with a system containing W_n rather than Z_n, so we divide (4.17) by $1 - Z_n$ to obtain

$$A_n^q(1 - iW_n) - iW_n \sum_{m=-\infty}^{\infty} \sum_{p=0}^{\infty} A_m^p S_{m-n}^{q-p}(k\cos\psi_0) = W_n i^{n+1} e^{i(q\mathbf{a}_2\cdot\mathbf{k} - n\psi_0)},$$
$$n \in \mathbb{Z}, \quad q = 0, 1, \ldots \quad (4.19)$$

This rescaling has no effect on the convergence properties of the system, because $1 - Z_n \to 1$ as $|n| \to \infty$. If there are integers n such that $Z_n = 1$, then no corresponding coefficient W_n exists for this index, but we can deal with this by introducing additional scaling factors into a finite number of rows. The effect of this scaling on subsequent analysis is minimal.

5. Exact Wiener–Hopf equation

We now convert (4.17) into a matrix Wiener–Hopf equation, using a generalisation of the method in (**11**), which was itself based on that in (**17**). We begin by setting

$$A_n^q = 0, \quad q < 0, \quad (5.1)$$

and

$$T_n^q = W_n i^{n+1} e^{i(q\mathbf{a}_2\cdot\mathbf{k} - n\psi_0)}, \quad q \geq 0, \quad (5.2)$$

so that (4.17) can be written in the form

$$A_n^q(1 - iW_n) - iW_n \sum_{m=-\infty}^{\infty} \sum_{p=-\infty}^{\infty} A_m^p S_{m-n}^{q-p}(k\cos\psi_0) = T_n^q, \quad n, q \in \mathbb{Z}. \quad (5.3)$$

At this stage, T_n^q is unknown for $q < 0$, but its physical meaning can be deduced by observing that an expansion of the total field in regular wavefunctions exists about every point except the cylinder centres. If we extend the definition of the vectors $\mathbf{R}_{jp}$ by allowing p to take any integer value, we can obtain such an expansion about $\mathbf{r} = \mathbf{R}_{0q}$ with $q < 0$ by setting $A_n^q = 0$ in (4.8), so that there is no field radiating from $\mathbf{r}_{0q} = \mathbf{0}$. Consequently, (4.8), (4.9) and (4.10) are extended to negative q by (5.1). By comparing (5.3) to (4.10), we see that

$$I_n^q = i^n e^{i(q\mathbf{a}_2\cdot\mathbf{k} - n\psi_0)} + iW_n^{-1} T_n^q, \quad q < 0. \quad (5.4)$$

The first term on the right-hand side of this equation originates from the expansion of the incident plane wave (4.4), meaning that the scattered field has the expansion

$$u^{\mathrm{s}}(\mathbf{r}) = i \sum_{n=-\infty}^{\infty} W_n^{-1} T_n^q \mathcal{J}_n(\mathbf{r}_{0q}), \quad q < 0, \quad (5.5)$$

which is valid in the vicinity of the point $\mathbf{r} = \mathbf{R}_{0q}$. An important consequence of this is that T_n^q cannot grow as $q \to -\infty$. We can also relate T_n^q to the coefficients in grating mode expansion by deriving Jacobi expansions of the form (4.4) for each term in (3.6). The result is that

$$u^{\mathrm{s}}(\mathbf{r}) = \sum_{j=-\infty}^{\infty} c_{j0}^{-} e^{iqk(\eta_1\cos\psi_j - \eta_2\sin\psi_j)} \sum_{n=-\infty}^{\infty} i^n e^{in\psi_j} \mathcal{J}_n(\mathbf{r}_{0q}), \quad (5.6)$$

and on comparing this to (5.5), we find that

$$T_n^q = W_n i^{n-1} \sum_{j=-\infty}^{\infty} c_{j0}^- e^{iqk(\eta_1 \cos\psi_j - \eta_2 \sin\psi_j)} e^{in\psi_j}, \quad q < 0. \tag{5.7}$$

Returning to the task of converting the system (4.17) to a Wiener–Hopf equation, we apply the z transform by introducing the integral representations

$$A_n^q = \frac{1}{2\pi i} \int_\Omega A_n^+(z) z^{-q-1}\, dz, \tag{5.8}$$

and

$$T_n^q = \frac{1}{2\pi i} \int_\Omega T_n(z) z^{-q-1}\, dz, \tag{5.9}$$

where Ω is an anticlockwise oriented simple closed contour encircling the origin, whose precise specification will be determined shortly. The superscript '+' denotes a function that is analytic inside Ω; its presence in (5.8) ensures that (5.1) is satisfied. In a similar way, we ensure that (5.2) is satisfied by writing

$$T_n(z) = T_n^+(z) + T_n^-(z), \tag{5.10}$$

where the superscript '−' denotes a function that is analytic outside Ω. Next, we choose

$$T_n^+(z) = -i^{n+1} e^{-in\psi_0} W_n \frac{\rho_0}{z - \rho_0}, \tag{5.11}$$

where

$$\rho_0 = e^{-i\mathbf{a}_2\cdot\mathbf{k}} = e^{-ik(\eta_1 \cos\psi_0 + \eta_2 \sin\psi_0)}, \tag{5.12}$$

and indent the contour Ω so that ρ_0 lies outside. A straightforward application of the residue theorem then shows that (5.2) is satisfied, provided that

$$T_n^-(z) \to 0 \quad \text{as} \quad z \to \infty. \tag{5.13}$$

The next step is to insert the integral representations (5.8) and (5.9) into (5.3), and evaluate the sum over p. Some care is needed here, to ensure correct positioning of the contour Ω relative to the singularities in the z plane. We begin by using (4.11) and (A.12) to obtain

$$S_n^q(k\cos\psi_0) = \begin{cases} \dfrac{2(-i)^n}{ka_1} \displaystyle\sum_{j=-\infty}^{\infty} \frac{e^{in\psi_j}}{\rho_j^q \sin\psi_j} & \text{if} \quad q > 0, \\[2ex] \dfrac{2(-i)^n}{ka_1} \displaystyle\sum_{j=-\infty}^{\infty} \frac{\tau_j^q e^{-in\psi_j}}{\sin\psi_j} & \text{if} \quad q < 0, \end{cases} \tag{5.14}$$

where ρ_j and τ_j are defined in terms of the scattering angles via

$$\rho_j = e^{-ik(\eta_1 \cos\psi_j + \eta_2 \sin\psi_j)} \quad \text{and} \quad \tau_j = e^{ik(\eta_1 \cos\psi_j - \eta_2 \sin\psi_j)}. \tag{5.15}$$

Note that the definition of ρ_j is consistent with (5.12) in the case where $j = 0$, and that $|\rho_j| = |\tau_j|$ grows exponentially as $|j| \to \infty$, in view of (3.2) and (3.3). For the terms in (5.3) with $p < q$, we use (5.14) to obtain

$$\sum_{p=-\infty}^{q-1} S_{m-n}^{q-p}(k\cos\psi_0)A_m^p = \frac{i^{n-m-1}}{\pi k a_1}\sum_{p=1}^{\infty}\sum_{j=-\infty}^{\infty}\frac{e^{i(m-n)\psi_j}}{\sin\psi_j}\int_\Omega A_m^+(z)(z/\rho_j)^p z^{-q-1}\,dz. \quad (5.16)$$

Since $A_m^+(z)$ is analytic inside Ω, we may temporarily contract the contour so that it includes only points at which $|z| < 1$, without changing the value of the integral. Since $|\rho_j| \geq 1$ for all j, the sum over p then converges exponentially, and on commuting this with the integral, we obtain

$$\sum_{p=-\infty}^{q-1} S_{m-n}^{q-p}(k\cos\psi_0)A_m^p = \frac{i^{n-m-1}}{\pi k a_1}\sum_{j=-\infty}^{\infty}\frac{e^{i(m-n)\psi_j}}{\sin\psi_j}\int_\Omega A_m^+(z)z^{-q}\frac{dz}{\rho_j - z}. \quad (5.17)$$

The poles that have been revealed at the points $z = \rho_j$ lie outside the contour Ω. Now the amplitude coefficients A_n^q cannot grow as $q \to \infty$, so the integral in (5.8) must not include contributions from singularities inside the unit circle, meaning that $A_n^+(z)$ is analytic for $|z| < 1$. However, this is not sufficient to deal with the terms in (5.3) with $p > q$. Therefore we temporarily assume the existence of $\epsilon > 0$ such that $A_n^+(z)$ is analytic for $|z| < 1 + \epsilon$. This means that $A_n^q \to 0$ as $q \to \infty$. Later we will see that a minor adjustment to the integration contour Ω allows our solution to hold in cases where Bloch waves are excited, and no such ϵ exists. Using (5.14) and temporarily expanding the contour Ω so that it does not include any points where $|z| \leq 1$, we find that

$$\sum_{p=q+1}^{\infty} S_{m-n}^{q-p}(k\cos\psi_0)A_m^p = \frac{i^{n-m-1}}{\pi k a_1}\sum_{j=-\infty}^{\infty}\frac{e^{i(n-m)\psi_j}}{\sin\psi_j}\int_\Omega A_m^+(z)z^{-q-1}\frac{dz}{z\tau_j - 1}. \quad (5.18)$$

The poles at the points $z = \tau_j^{-1}$ lie inside the contour Ω. Using (5.17) and (5.18) in (5.3), and using (5.8) and (5.9) for the remaining terms, we now find that a solution is obtained if

$$\sum_{m=-\infty}^{\infty} K_{nm}(z)A_m^+(z) = T_n^+(z) + T_n^-(z), \quad n \in \mathbb{Z}, \quad (5.19)$$

where the element of the kernel matrix in row n and column m is given by

$$K_{nm}(z) = \delta_{nm} - i\,W_n\left(\sigma_{n-m} + \delta_{nm} - \frac{2i^{n-m}}{ka_1}\sum_{j=-\infty}^{\infty}\frac{1}{\sin\psi_j}\left[\frac{ze^{i(m-n)\psi_j}}{z-\rho_j} - \frac{e^{i(n-m)\psi_j}}{z\tau_j - 1}\right]\right). \quad (5.20)$$

Here, we have omitted the argument $k\cos\psi_0$ from σ_{n-m} for brevity. The contour Ω is shown in Fig. 2. It consists of the unit circle, with indentations chosen so that the points $z = \tau_j^{-1}$ are encircled, but the points $z = \rho_j$ are not. The system (5.19) is an infinite-dimensional matrix Wiener–Hopf equation, though as noted in the previous section the ranges for n and m can be truncated. Each element of the matrix kernel has infinitely many simple

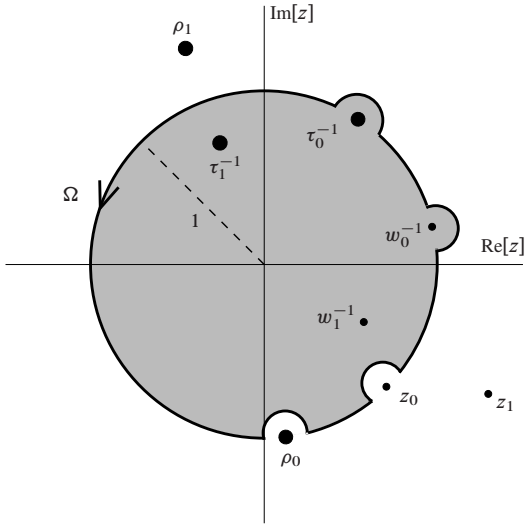

Fig. 2 Schematic diagram showing the contour Ω, the poles ρ_0, ρ_1, τ_0^{-1} and τ_1^{-1} and the zeros of the kernel z_0, z_1, w_0^{-1} and w_1^{-1}. When $j \in \mathcal{N}$, $\rho_j^* = \tau_j$ and similarly, $z_j = w_j^*$ if $|z_j| \neq 1$. Functions with a superscript + (−) are analytic in the (un)shaded region.

poles. Since $|\rho_j| = |\tau_j| \to \infty$ as $j \to \infty$, there are also nonisolated essential singularities caused by the clustering of poles about the origin and the point at infinity. A final point concerns the Wood anomalies studied in (**25**). These are situations in which there exist one or two integers j such that $\sin\psi_j = 0$. Inserting the spectral form of σ_{n-m} from equation (B.4) or (B.5) into (5.20), and using Euler's formula shows that $K_{nm}(z)$ remains bounded in the limit $\sin\psi_j \to 0$. Consequently, Wood anomalies have no significant effect on our subsequent analysis, though some care is needed in order to obtain the correct values for $K_{nm}(z)$ in such cases.

6. Symmetries

In this section, we prove the crucial symmetry property

$$W_n^{-1} K_{nm}(z) = W_m^{-1} K_{mn}^*(1/z^*), \tag{6.1}$$

where the superscript '$*$' denotes the complex conjugate. To achieve this, we will show that

$$\mathsf{D}_{nm} = W_n^{-1} K_{nm}(z) - W_m^{-1} K_{mn}^*(1/z^*) \tag{6.2}$$

is identically zero. Now the first term on the right-hand of (5.20) clearly disappears from (6.2). For the second term, we observe that when $n = m$ the Kronecker delta eliminates the first term in the spectral form of σ_0 (B.4). In this case, the second term from (B.4) also disappears from (6.2), as does the contribution $i/(\pi|j|)$ in the summand, due to the addition of σ_0^* to σ_0. Similarly, when $m \neq n$, we use (B.2) to equate the orders of the two Schlömilch series in (6.2), and then the term $\mathcal{B}_n$ from (B.5) disappears. Only the infinite sum over j remains,

and in fact

$$\mathsf{D}_{nm} = -\frac{2i^{n-m+1}}{ka_1}\sum_{j=-\infty}^{\infty}\mathsf{D}^j_{nm}, \tag{6.3}$$

where

$$\mathsf{D}^j_{nm} = \frac{1}{\sin\psi_j}\left[e^{i(n-m)\,\mathrm{sgn}(j)\psi_j} - \frac{ze^{i(m-n)\psi_j}}{z-\rho_j} + \frac{e^{i(n-m)\psi_j}}{z\tau_j - 1}\right] + \frac{1}{\sin\psi^*_j}\left[e^{i(m-n)\,\mathrm{sgn}(j)\psi^*_j} - \frac{ze^{i(n-m)\psi^*_j}}{z-\tau^*_j} + \frac{e^{i(m-n)\psi^*_j}}{z\rho^*_j - 1}\right], \tag{6.4}$$

and $\mathrm{sgn}(0) = 1$. When $\sin\psi_j$ is imaginary, $\rho^*_j = \tau_j$ and (3.2) shows that either $\psi_j = iv$ or $\psi_j = \pi - iv$, with $v > 0$. On the other hand, if ψ_j is real, both ρ_j and τ_j lie on the unit circle, so that $\rho^*_j = 1/\rho_j$ and $\tau^*_j = 1/\tau_j$. In either case, it immediately follows that $\mathsf{D}^j_{nm} = 0$, which establishes (6.1).

Another symmetry property,

$$(-1)^n W_n^{-1} K_{nm}(z) = (-1)^m W_m^{-1} K_{mn}(1/z), \tag{6.5}$$

holds only in the case of a rectangular lattice, where $\eta_1 = 0$ so that $\rho_j = \tau_j$, and a third,

$$(-1)^n W_n^{-1} K_{nm}(z) = (-1)^m W_m^{-1} K_{mn}\left(\frac{1}{ze^{ika_1\cos\psi_0}}\right), \tag{6.6}$$

holds only if $\eta_1 = a_1/2$, so that $\tau_j = e^{ika_1\cos\psi_0}\rho_j$. These are easily verified by taking the difference between the left- and right-hand sides and using (5.20). Both (6.5) and (6.6) have previously been obtained in (**26**). On the other hand, the general symmetry property (6.1) was observed numerically in (**26**) but not proven.

7. Approximate Wiener–Hopf equation

In order to proceed further, we introduce two approximations into the matrix Wiener–Hopf equation (5.19). First, the system is truncated at $|m| = |n| = N$. This corresponds to using a finite number of wavefunctions in the expansions of the field about the cylinders. As noted in Section 2, accurate results can be obtained for relatively small values of N, due to rapid convergence. We also truncate the sum over j in (5.20). The physical meaning of this can be understood as follows. First of all, note that the sum in question originates from the use of the spectral representations of the function S^{q-p}_{m-n} in obtaining (5.19) from (5.3). The terms in which $q = p$ describe the interactions between the scatterers within each row; hence the appearance of the Schlömilch series σ_{n-m}, the exact form of which is retained in our approximation. On the other hand, terms in which $q \neq p$ describe interactions between distinct rows, and, in view of (A.12), these interactions are due to an infinite sum of grating modes propagating between the rows. All but a finite number of these modes are evanescent, and the rate of decay increases rapidly with the modulus of the summation index j. It is this sum which we are now truncating, thereby discarding interaction effects caused by strongly damped modes, and so in fact the approximation amounts to a standard method

for treating scattering by multiple linear arrays (see (**15**, Section 6.4), (**27**) and references therein). The $(2N+1)\times(2N+1)$ approximate Wiener–Hopf equation is therefore

$$\mathbf{K}(z)\mathbf{A}^{+}(z)=\mathbf{T}(z), \tag{7.1}$$

where the entries in row n of the vectors $\mathbf{A}^{+}(z)$ and $\mathbf{T}(z)$ are $A_n^{+}(z)$ and $T_n(z)$, respectively, and the entry in row n and column m of the matrix $\mathbf{K}(z)$ is

$$\tilde{K}_{nm}(z)=\delta_{nm}-iW_n\biggl(\sigma_{n-m}+\delta_{nm}-\frac{2i^{n-m}}{ka_1}\sum_{j=j_0}^{j_1}\frac{1}{\sin\psi_j}\biggl[\frac{ze^{i(m-n)\psi_j}}{z-\rho_j}-\frac{e^{i(n-m)\psi_j}}{z\tau_j-1}\biggr]\biggr). \tag{7.2}$$

The truncation parameters j_0 and j_1 must be such that no propagating modes are discarded, and so the summation must include all elements of the set $\mathcal{M}$, but it may also be necessary to include one or more evanescent modes, depending on the rate of decay and the degree of accuracy required. This second approximation eliminates the essential singularities from the origin and the point at infinity, so that $\tilde{K}_{nm}(z)$ is a rational function with $2(j_1-j_0+1)$ simple poles. The residues at these poles are exactly those of $K_{nm}(z)$. The approximate kernel matrix has the same symmetry properties as the exact matrix (see Section 6), because in each case the symmetry applies to individual terms in the sum over j. In the case of (6.1), it should be noted that the terms in (6.4) originating from σ_{n-m} cancel each other for $j\in\mathcal{N}$, meaning that the Schlömilch series need not (and indeed should not) be truncated in the same way.

The usual method for solving equations such as (7.1) requires a factorisation of the form

$$\mathbf{K}(z)=\mathbf{K}^{+}(z)\mathbf{K}^{-}(z), \tag{7.3}$$

where $\det\mathbf{K}^{+}(z)\neq 0$ for all z on and inside the contour Ω. Such factorisations are often very difficult to find (**21**). Here, we can avoid this problem by exploiting the fact that the Wiener–Hopf equation contains only rational functions. This allows us to construct the functions $T_n^{-}(z)$ by matching the poles and residues on each side of (7.1) (or, equivalently, the truncated form of (5.19)). The procedure we use is related to the method introduced in (**28**), though in that case the equation is simpler in that the right-hand side is known and the difficulty lies in determining the residues in the unknown vector on the left-hand side. To begin the construction, we simply observe that $A_m^{+}(z)$ and $T_n^{-}(z)$ cannot have common singularities, so the only possible singularities of $T_n^{-}(z)$ are the poles of the kernel that lie outside the contour Ω. Consequently, $T_n^{-}(z)$ has at most simple poles at the points $z=\tau_j^{-1}$, and no other singularities. Recalling that $T_n^{-}(z)\to 0$ as $z\to\infty$, we immediately obtain the expansion

$$T_n^{-}(z)=W_n\sum_{j=j_0}^{j_1}\frac{X_n^j}{z\tau_j-1}, \tag{7.4}$$

where the coefficients X_n^j are as yet unknown, and the factor W_n has been included for convenience, and consistency with (5.11). A remarkable simplification now occurs if we multiply (7.2) by $z\tau_p-1$ with $j_0\leq p\leq j_1$ and take the limit $z\to\tau_p^{-1}$. We find that

$$\lim_{z\to\tau_p^{-1}}\bigl[(z\tau_p-1)\tilde{K}_{nm}(z)\bigr]=-\frac{2i^{1-m}e^{-im\psi_p}}{ka_1\sin\psi_p}W_ni^ne^{in\psi_p}, \tag{7.5}$$

and since $T_n^+(z)$ is analytic at the points $z = \tau_p^{-1}$, using this in the truncated form of (5.19) shows that

$$X_n^p = -\frac{2i^{n+1}e^{in\psi_p}}{ka_1 \sin\psi_p} \sum_{m=-N}^{N} A_m^+(\tau_p^{-1})(-i)^m e^{-im\psi_p}, \tag{7.6}$$

which reveals the dependence of X_n^p on n. In fact

$$X_n^p = i^n e^{in\psi_p} X_0^p, \tag{7.7}$$

so that (7.4) becomes

$$T_n^-(z) = i^n W_n \sum_{j=j_0}^{j_1} \frac{X_0^j e^{in\psi_j}}{z\tau_j - 1}, \tag{7.8}$$

and it only remains to determine the coefficients X_0^j.

Next, we define the determinant function

$$d(z) = \det \mathbf{K}(z), \tag{7.9}$$

which is a rational function that is analytic except possibly for poles located at $z = \rho_j$ and $z = \tau_j^{-1}$, for $j = j_0, \ldots, j_1$. Consider the point $z = \tau_p^{-1}$. From (7.5), we have

$$\operatorname*{Res}_{z=\tau_p^{-1}} \big[\tilde{K}_{nm}(z)\big] = \frac{W_n}{W_0} i^n e^{in\psi_p} \operatorname*{Res}_{z=\tau_p^{-1}} \big[\tilde{K}_{0m}(z)\big], \tag{7.10}$$

which shows that the residues in row n of the kernel matrix elements differ from those in row 0 by a common, constant factor. The residues at $z = \rho_p$ are related in a similar way, with $e^{in\psi_p}$ replaced by $e^{-in\psi_p}$. Motivated by this, we define the regularised kernel matrix $\mathbf{L}(z)$, whose elements are given by

$$L_{nm}(z) = \begin{cases} \tilde{K}_{0m}(z) & \text{if } n = 0, \\ \tilde{K}_{nm}(z) - \dfrac{W_n}{W_0} i^n e^{\mp in\psi_p} \tilde{K}_{0m}(z) & \text{otherwise,} \end{cases} \tag{7.11}$$

for $|m| \le N$ and $|n| \le N$. Evidently the determinant of $\mathbf{L}(z)$ is the same as that of $\mathbf{K}(z)$, but by making the appropriate choice of the index p and the sign in the exponent, any one of the poles can be removed identically from all but one of the rows. This shows that $d(z)$ can have (at most) simple poles at the points $z = \rho_j$ and $z = \tau_j^{-1}$. Furthermore, it follows from the symmetry property (6.1) that

$$d(z) = d^*(1/z^*). \tag{7.12}$$

Any rational function with this property must be a ratio of polynomials of equal degree. We will proceed on the basis that the zeros of $d(z)$ are simple, and do not coincide with the poles at $z = \rho_j$ and $z = \tau_j^{-1}$, which has been the case for every parameter set we have considered. Since we have not discovered any mathematical arguments that preclude other possibilities such as higher order zeros, some modifications to our analysis that can be used in such situations are presented in appendix C. Now the zeros of $d(z)$ are subject to the

symmetry relation (7.12), and initially we will assume that $d(z)$ has no zeros on the unit circle. In this case, there are $(j_1 - j_0 + 1)$ zeros z_p outside the unit circle, and for each of these there is a corresponding zero located at $z = w_p^{-1} = 1/z_p^*$, which lies inside the unit circle. Zeros of $d(z)$ that lie outside the unit circle correspond to poles of $A_n^+(z)$. On the other hand, $A_n^+(z)$ is analytic at the points $z = w_p^{-1}$ and here the Fredholm alternative (**29**, Sections 5.7–5.9) imposes a condition on the right-hand side of (7.1). Specifically, there exists a nonzero vector $\mathbf{E}_p$ such that

$$\mathbf{K}^*(w_p^{-1})\mathbf{E}_p = \mathbf{0}, \tag{7.13}$$

and it must be the case that

$$\mathbf{E}_p^*\mathbf{T}(w_p^{-1}) = 0. \tag{7.14}$$

When the superscript '$*$' is applied to a matrix or vector, it denotes a conjugate transpose. Substituting $T_n^+(z)$ from (5.11) and the truncated form of $T_n^-(z)$ from (7.8), we can write this in explicit form. If the row vector $\mathbf{E}_p^*$ has entries E_{pn}^*, for $n = -N, \ldots, N$, then

$$\sum_{j=j_0}^{j_1} \frac{X_0^j}{w_p^{-1}\tau_j - 1} \sum_{n=-N}^{N} W_n E_{pn}^* i^n e^{in\psi_j} = \frac{i\rho_0}{w_p^{-1} - \rho_0} \sum_{n=-N}^{N} W_n E_{pn}^* i^n e^{-in\psi_0}, \quad p = j_0, \ldots, j_1. \tag{7.15}$$

This determines X_0^j. If one or more of the points w_p lies on the unit circle, then the corresponding points z_p must also lie on the unit circle, or else the symmetry property (7.12) cannot be satisfied. Contributions to A_n^p from poles on the unit circle do not decay as $p \to \infty$; these correspond to Bloch waves in the far field. When a pair of zeros occurs on the unit circle, we must determine the direction in which the corresponding Bloch waves transport energy across lines where y is constant (see Section 10 for details). One zero in each pair corresponds to a Bloch wave which carries energy into the lattice, and we denote this zero by z_p. The other zero in the pair corresponds to a wave that is incoming from the far field, and cannot be excited by a wave incident from below the lattice. We denote this zero by w_p^{-1}; it cannot be a pole of $A_n^+(z)$. Once the zeros are classified in this way, we indent Ω so that w_p^{-1} is encircled, but z_p is not (Fig. 2). This done, (7.15) can be used to determine X_0^j as before.

8. The far field

Having constructed the functions $T_n^-(z)$, and thereby determined $A_n^+(z)$, we now turn our attention to the behaviour of the scattered field. The method we use for the analysis in this section was developed in (**11**). We begin by expressing the multipole representation (4.1) in terms of the quasi-periodic Green's function (A.1) and using the integral representation for A_n^p (5.8); thus

$$u^{\mathrm{s}}(\mathbf{r}) = \frac{1}{2\pi i} \sum_{n=-N}^{N} \sum_{p=0}^{\infty} \int_{\Omega} A_n^+(z) z^{-p-1}\, dz\, G_n(\mathbf{r} - p\mathbf{a}_2, k\cos\psi_0). \tag{8.1}$$

The next step is to expand Ω into a new contour Ω' which does not include any points where $|z| \leq 1$, thereby causing the sum over p to converge exponentially. Clearly, this process is

impeded by poles of $A_n^+(z)$ that lie on the unit circle. We will assume that there is one such pole at the point $z = z_0$. Contributions from additional poles can be included in exactly the same way, and for the case where $A_n^+(z)$ is analytic on the unit circle, we simply set $b = 0$ in our subsequent analysis. The functions $A_n^+(z)$ cannot include contributions from poles on the unit circle that are not simple. This follows from (5.8), and the fact that if $f(z_0) \neq 0$, then

$$\operatorname{Res}\left[\frac{f(z)z^p}{(z-z_0)^2}\right] = f'(z_0)z^p + f(z_0)\,pz_0^{p-1}, \tag{8.2}$$

and similarly for higher order poles. Since the second term grows as $p \to \infty$, such a residue leads to unphysical results. Therefore we may write

$$\mathbf{A}^+(z) = \frac{b\mathbf{B}}{z-z_0} + \hat{\mathbf{A}}^+(z), \tag{8.3}$$

where $\hat{\mathbf{A}}^+(z)$ is analytic at $z = z_0$ and $|\mathbf{B}| = 1$. The residue term corresponds to a Bloch wave in the far-field. The vector $\mathbf{B}$ describes the form of this wave, and the scalar b determines its amplitude. If we substitute (8.3) into the approximate Wiener–Hopf equation (7.1), multiply by $z - z_0$ and take the limit $z \to z_0$, we find that

$$\mathbf{K}(z_0)\mathbf{B} = \mathbf{0}, \tag{8.4}$$

which determines $\mathbf{B}$, up to a factor ± 1. Taking the residue term to the right-hand side of (7.1) yields

$$\mathbf{K}(z)\hat{\mathbf{A}}^+(z) = \mathbf{T}(z) - \frac{b\mathbf{K}(z)\mathbf{B}}{z-z_0} \tag{8.5}$$

and we can now apply the Fredholm alternative to obtain an expression for b. Thus, there exists a vector $\mathbf{F}$ such that $|\mathbf{F}| = 1$ and

$$\mathbf{K}^*(z_0)\mathbf{F} = \mathbf{0}, \tag{8.6}$$

and after left-multiplying (8.5) by $\mathbf{F}^*$, taking the limit $z \to z_0$ and applying L'Hôpital's rule, we find that

$$\mathbf{F}^*\mathbf{T}(z_0) = b\mathbf{F}^*\mathbf{K}'(z_0)\mathbf{B}, \tag{8.7}$$

where the prime denotes differentiation of each individual matrix element with respect to z. Since z_0 lies on the unit circle, we may replace z_0 with $1/z_0^*$ in (8.6), and the symmetry property (6.1) shows that the elements of $\mathbf{F}$ are related to those of $\mathbf{B}$ via $W_n F_n = \pm B_n$.

Deforming the contour of integration in (8.1) and collecting the residue at $z = z_0$ yields

$$u^{\mathrm{s}}(\mathbf{r}) = u_1^{\mathrm{b}}(\mathbf{r}) + \frac{1}{2\pi i}\sum_{n=-N}^{N}\sum_{p=0}^{\infty}\int_{\Omega'} A_n^+(z)z^{-p-1}\,dz\,G_n(\mathbf{r} - p\mathbf{a}_2, k\cos\psi_0), \tag{8.8}$$

where

$$u_1^{\mathrm{b}}(\mathbf{r}) = -\frac{b}{z_0}\sum_{n=-N}^{N} B_n \sum_{p=0}^{\infty} z_0^{-p} G_n(\mathbf{r} - p\mathbf{a}_2, k\cos\psi_0). \tag{8.9}$$

We can evaluate the sum over p by choosing λ_0 so that

$$z_0 = e^{-ia_2\cdot\boldsymbol{\beta}_0} \quad \text{with} \quad \boldsymbol{\beta}_0 = k\cos\psi_0\hat{\mathbf{x}} + \lambda_0\hat{\mathbf{y}}. \tag{8.10}$$

We then have a sum of the form (A.5), and so

$$u_1^{\mathrm{b}}(\mathbf{r}) = -\frac{b}{z_0}\sum_{n=-N}^{N} B_n G_n^{(0,\infty)}(\mathbf{r},\boldsymbol{\beta}_0). \tag{8.11}$$

Next, we convert the Green's function in (8.8) to spectral form using (A.12), and in this way we obtain

$$u^{\mathrm{s}}(\mathbf{r}) = u_1^{\mathrm{b}}(\mathbf{r}) + \sum_{n=-N}^{N}(-i)^{n+1}\sum_{p=0}^{\infty}\int_{\Omega'} A_n^+(z)z^{-p-1}\,dz \sum_{j=-\infty}^{\infty}\frac{e^{in\,\mathrm{sgn}(y-p\eta_2)\psi_j}}{\pi k a_1\sin\psi_j} \times e^{ik((x-p\eta_1)\cos\psi_j+|y-p\eta_2|\sin\psi_j)}. \tag{8.12}$$

To proceed beyond this point we must evaluate the sum over p, and this in turn requires the elimination of the modulus and signum functions. Clearly, this is immediate if $y<0$, but the case where $y>0$ is more difficult. Setting $y=(P+t)\eta_2$, with $0<t<1$, we find that

$$u^{\mathrm{s}}(\mathbf{r}) = u_1^{\mathrm{b}}(\mathbf{r}) + \sum_{n=-N}^{N}\frac{(-i)^{n+1}}{\pi k a_1}\sum_{j=-\infty}^{\infty}\frac{e^{ikx\cos\psi_j}}{\sin\psi_j}\int_{\Omega'}\frac{A_n^+(z)}{z} \times\left[e^{ik(P+t)\eta_2\sin\psi_j}e^{in\psi_j}\sum_{p=0}^{P}\left(\frac{\rho_j}{z}\right)^p + e^{-ik(P+t)\eta_2\sin\psi_j}e^{-in\psi_j}\sum_{p=P+1}^{\infty}(z\tau_j)^{-p}\right]dz, \tag{8.13}$$

where ρ_j and τ_j are given by (5.15). Since $|z|>1$ on Ω' and $|\tau_j|\geq 1$ for all $j\in\mathbb{Z}$, we may now evaluate both geometric series, and this yields

$$u^{\mathrm{s}}(\mathbf{r}) = u_1^{\mathrm{b}}(\mathbf{r}) + \sum_{n=-N}^{N}\frac{(-i)^{n+1}}{\pi k a_1}\sum_{j=-\infty}^{\infty}\frac{e^{ikx\cos\psi_j}}{\sin\psi_j}\int_{\Omega'}A_n^+(z)\left[e^{ik(P+t)\eta_2\sin\psi_j}\frac{e^{in\psi_j}}{z-\rho_j} - z^{-P-1}e^{-ikP\eta_1\cos\psi_j}\left(e^{ikt\eta_2\sin\psi_j}\frac{\rho_j e^{in\psi_j}}{z-\rho_j} - e^{-ikt\eta_2\sin\psi_j}\frac{e^{-in\psi_j}}{\tau_j z-1}\right)\right]dz. \tag{8.14}$$

Taking the limit $P\to\infty$ now eliminates the last two terms on the right-hand side and reduces the range for j to elements of the set $\mathcal{M}$ only; hence

$$u^{\mathrm{s}}(\mathbf{r}) \sim u_1^{\mathrm{b}}(\mathbf{r}) + \sum_{n=-N}^{N}\frac{(-i)^{n+1}}{\pi k a_1}\sum_{j\in\mathcal{M}}\frac{e^{in\psi_j}}{\sin\psi_j}e^{ik(x\cos\psi_j+y\sin\psi_j)}\int_{\Omega'}A_n^+(z)\frac{dz}{z-\rho_j}. \tag{8.15}$$

There are now two poles inside the contour of integration, at $z=\rho_j$ and $z=z_0$, so after applying the residue theorem we have

$$u^{\mathrm{s}}(\mathbf{r}) \sim u_1^{\mathrm{b}}(\mathbf{r}) + u_2^{\mathrm{b}}(\mathbf{r}) + \sum_{j\in\mathcal{M}}\frac{2e^{ik(x\cos\psi_j+y\sin\psi_j)}}{ka_1\sin\psi_j}\sum_{n=-N}^{N}(-i)^n e^{in\psi_j}A_n^+(\rho_j), \tag{8.16}$$

where

$$u_2^{\mathrm{b}}(\mathbf{r}) = \frac{2b}{ka_1} \sum_{n=-N}^{N} (-i)^n B_n \sum_{j \in \mathcal{M}} \frac{e^{in\psi_j} e^{ik(x\cos\psi_j + y\sin\psi_j)}}{\sin\psi_j (z_0 - \rho_j)}, \tag{8.17}$$

having used (8.3) again to evaluate the contribution at $z = z_0$. The sum over n in (8.16) can be evaluated by multiplying the truncated form of (5.19) by $z - \rho_q$ and taking the limit $z \to \rho_q$. Since $\mathbf{T}^-(z)$ is analytic at $z = \rho_q$, this term disappears, and we can use (5.11) and (7.2) to obtain

$$u^{\mathrm{s}}(\mathbf{r}) \sim u_1^{\mathrm{b}}(\mathbf{r}) + u_2^{\mathrm{b}}(\mathbf{r}) - e^{ik(x\cos\psi_0 + y\sin\psi_0)}, \tag{8.18}$$

so that the last term cancels the incident field. Finally, we observe that (8.17) is in fact the far field pattern generated by a combination of quasi-periodic Green's functions of the form (A.20). Indeed,

$$-\frac{b}{z_0} \sum_{n=-N}^{N} B_n G_n^{(-\infty,-1)}(\mathbf{r}, \boldsymbol{\beta}_0) \sim u_2^{\mathrm{b}}(\mathbf{r}) \tag{8.19}$$

as $y \to \infty$, so that the total field has the asymptotic form

$$u(\mathbf{r}) \sim -\frac{b}{z_0} \sum_{n=-N}^{N} B_n G_n^{(-\infty,\infty)}(\mathbf{r}, \boldsymbol{\beta}_0), \tag{8.20}$$

which is a Bloch wave.

Calculation of the reflected field is much more straightforward. Setting $y < 0$ in (8.12) and evaluating the sum over p yields

$$u^{\mathrm{s}}(\mathbf{r}) = u_1^{\mathrm{b}}(\mathbf{r}) + \sum_{n=-N}^{N} \frac{(-i)^{n+1}}{\pi k a_1} \sum_{j=-\infty}^{\infty} \frac{e^{-in\psi_j}}{\sin\psi_j} e^{ik(x\cos\psi_j - y\sin\psi_j)} \int_{\Omega'} A_n^+(z) \frac{\tau_j \, dz}{\tau_j z - 1}. \tag{8.21}$$

If we now write u_1^{b} explicitly using (8.11) and (A.19), and take the residue at $z = z_0$ using (8.3), we find that these two terms cancel each other exactly, so that we are left with the grating mode expansion (3.6), with

$$c_{j0}^- = \frac{2}{ka_1 \sin\psi_j} \sum_{n=-N}^{N} (-i)^n e^{-in\psi_j} A_n^+(\tau_j^{-1}). \tag{8.22}$$

Finally, the sum over n can be evaluated by setting $n = 0$ in (7.6); the result is that

$$c_{j0}^- = i X_0^j. \tag{8.23}$$

9. Conservation of energy

The energy flux carried across a contour $\mathcal{S}$ by the total field during one time period is given by the line integral

$$\langle E_{\mathcal{S}} \rangle = -\frac{P_0 \omega}{2} \operatorname{Im} \int_{\mathcal{S}} u(\mathbf{r}) \frac{\partial}{\partial n} u^*(\mathbf{r}) \, ds, \tag{9.1}$$

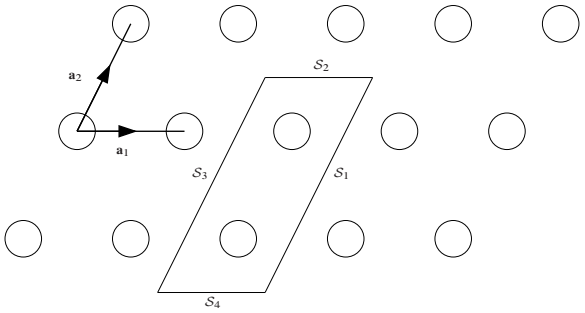

Fig. 3 The contour $\mathcal{S}$, composed of the four lines $\mathcal{S}_1, \ldots, \mathcal{S}_4$.

where P_0 is the quiescent fluid pressure and the orientation of the derivative is normal to $\mathcal{S}$; see (**11**) for details. If $\langle E_{\mathcal{S}} \rangle > 0$, the net energy flux is in the direction of the normal, whereas energy is transported in the opposite direction if $\langle E_{\mathcal{S}} \rangle < 0$. We choose $\mathcal{S}$ to be the parallelogram with vertices located at

$$\mathbf{r} = \tfrac{1}{2}\big(-\mathbf{a}_2 \pm \mathbf{a}_1\big) \quad \text{and} \quad \mathbf{r} = \big(q - \tfrac{1}{2}\big)\mathbf{a}_2 \pm \tfrac{1}{2}\mathbf{a}_1, \tag{9.2}$$

and take the derivative in the direction of the outgoing normal from each side. Since $\mathcal{S}$ is a closed contour, we then have $\langle E_{\mathcal{S}} \rangle = 0$, which amounts to conservation of energy. This result can also be obtained by applying Green's second identity (**14**, Section 6.5) to the total field and its complex conjugate. Next, we divide $\mathcal{S}$ into four straight line sections $\mathcal{S}_1, \ldots, \mathcal{S}_4$, as shown in Fig. 3. The quasi-periodicity relation (2.12) shows that the only difference between the integrals along $\mathcal{S}_1$ and $\mathcal{S}_3$ is due to the direction of the outgoing normal, so if we define

$$\mathrm{I}_v = -\frac{P_0\omega}{2}\,\mathrm{Im}\int_{\mathcal{S}_v} u(\mathbf{r})\frac{\partial}{\partial n}u^*(\mathbf{r})\,ds, \tag{9.3}$$

then we immediately see that

$$\mathrm{I}_1 + \mathrm{I}_3 = 0, \tag{9.4}$$

meaning energy is conserved if and only if

$$\mathrm{I}_2 + \mathrm{I}_4 = 0. \tag{9.5}$$

On $\mathcal{S}_2$ and $\mathcal{S}_4$, we use the grating mode representation (3.1), since evaluation of the two remaining integrals is then very straightforward. Indeed, it follows from (3.2) that

$$\int_{x_0-a_1/2}^{x_0+a_1/2} e^{ikx(\cos\psi_j - \cos\psi_p)}\,dx = a_1\delta_{jp}, \tag{9.6}$$

where x_0 may be chosen arbitrarily. Therefore, if u is given by (3.1), then

$$\int_{\mathcal{S}_v} u(\mathbf{r})\frac{\partial}{\partial n}u^*(\mathbf{r})\,ds = \mp ika_1 \sum_{j=-\infty}^{\infty} \sin\psi_j^*\big[c_j^+ e^{iky\sin\psi_j} + c_j^- e^{-iky\sin\psi_j}\big] \times \big[(c_j^+)^* e^{-iky\sin\psi_j^*} - (c_j^-)^* e^{iky\sin\psi_j^*}\big], \tag{9.7}$$

where $v = 2$ or $v = 4$, and the upper and lower signs correspond to an upwards or downwards oriented normal, respectively. Considerable simplification now occurs on separating the terms for which $\sin\psi_j$ is real from the remainder of the series, and taking the imaginary part. We find that

$$\mathrm{Im}\int_{\mathcal{S}_v} u(\mathbf{r})\frac{\partial}{\partial n}u^*(\mathbf{r})\,ds = \mp ka_1\sum_{j\in\mathcal{M}'}\sin\psi_j\big(|c_j^+|^2-|c_j^-|^2\big)\pm 2ka_1\sum_{j\in\mathcal{N}}|\sin\psi_j|\,\mathrm{Im}[c_j^+(c_j^-)^*], \tag{9.8}$$

where $\mathcal{N}$ is defined in (3.4), and $\mathcal{M}'$ is the set of integers j such that $|\cos\psi_j|<1$, so that terms with $\sin\psi_j = 0$ (which do not depend on y) are omitted. On $\mathcal{S}_4$, the outgoing normal is directed downwards, and the only upwards propagating mode is the incident field, so that $c_j^+ = \delta_{j0}$. The coefficients c_{j0}^- are given by (8.23), and with these we obtain

$$\mathrm{I}_4 = -\frac{ka_1}{2}P_0\omega\Big(\sin\psi_0 - \sum_{j\in\mathcal{M}'}\big|X_0^j\big|^2\sin\psi_j\Big). \tag{9.9}$$

There are two possibilities for the integral along $\mathcal{S}_2$. If no Bloch wave is excited, then the total field decays exponentially as $y\to\infty$, so we may take the limit $q\to\infty$ in the parametrisation (9.2) to show that $\mathrm{I}_2 = 0$. If a Bloch wave is excited due to a pole at $z = z_0$, then the far field for $y > 0$ is given by (8.20). In view of the quasiperiodicity property (A.17), this can be rewritten as

$$u(\mathbf{r}) \sim -\frac{b}{z_0}\,e^{i\mathbf{R}_{0q}\cdot\boldsymbol{\beta}_0}\sum_{n=-N}^{N}B_nG_n^{(-\infty,\infty)}(\mathbf{r}-q\mathbf{a}_2,\boldsymbol{\beta}_0). \tag{9.10}$$

For $\mathbf{r}\in\mathcal{S}_2$, we can use (A.19) and (A.20) to express this as a grating mode expansion of the form (3.5), with

$$c_{jq}^+ = -\frac{2b\,Q_j^+\rho_j^q e^{i\mathbf{R}_{0q}\cdot\boldsymbol{\beta}_0}}{ka_1\sin\psi_j(\rho_j-z_0)} \quad\text{and}\quad c_{jq}^- = \frac{2b\,Q_j^-\tau_j^{-q}e^{i\mathbf{R}_{0q}\cdot\boldsymbol{\beta}_0}}{ka_1\sin\psi_j(\tau_j^{-1}-z_0)}. \tag{9.11}$$

Here, $\boldsymbol{\beta}_0$ is given by (8.10), and

$$Q_j^\pm = \sum_{n=-\infty}^{\infty}(-i)^nB_ne^{\pm in\psi_j}. \tag{9.12}$$

Hence, (9.8) now yields

$$\mathrm{I}_2 = \frac{2|b|^2}{ka_1}P_0\omega\big(\mathrm{I}_2^{\mathcal{M}}+\mathrm{I}_2^{\mathcal{N}}\big), \tag{9.13}$$

where

$$\mathrm{I}_2^{\mathcal{M}} = \sum_{j\in\mathcal{M}'}\frac{1}{\sin\psi_j}\left(\left|\frac{Q_j^+}{\rho_j-z_0}\right|^2-\left|\frac{Q_j^-}{\tau_j^{-1}-z_0}\right|^2\right) \tag{9.14}$$

and

$$\mathrm{I}_2^{\mathcal{N}} = \sum_{j\in\mathcal{N}} \frac{-2}{|\sin\psi_j|}\,\mathrm{Im}\left[\frac{\rho_j z_0}{(\rho_j - z_0)^2}\,Q_j^+(Q_j^-)^*\right]. \tag{9.15}$$

Equation (9.13) is valid only for single Bloch waves, and the relationship between I_2 for individual and multiple waves is not linear. In cases where multiple Bloch waves are excited, the total amplitude of the grating modes should be calculated by summing the values given by (9.11) for each Bloch wave, and I_2 can then be evaluated using (9.8). The value for q in (9.11) may be chosen arbitrarily.

10. Implementation

The most significant obstacle to implementing the method described above is the determination of the points at which $d(z) = 0$. The general symmetry relation (6.1) means we need only locate those zeros that lie on or inside the unit circle, but the presence of poles at $z = \rho_j$ and $z = \tau_j^{-1}$ in every element of the kernel matrix and the fact that the determinant has only simple poles at these points means there is a danger of catastrophic cancellation if $d(z)$ is computed directly from (7.2). Any numerical code that operates on this basis is likely to be unstable. Indeed, even searching for zeros on the unit circle, where the determinant is real, is problematic because computed values of $d(z)$ close to the poles sometimes turn out to have the wrong sign. When very few terms are retained in the approximate kernel, it is possible to use a computer algebra package to expand and simplify the determinant, but this rapidly becomes unfeasible as the magnitudes of the truncation parameters are increased. Instead, we overcome this problem by computing the determinant using the regularised matrix $\mathbf{L}(z)$ and, for a given z, we choose the index p and the sign in (7.11) so as to reduce the order of the closest pole. Where advantageous, we multiply the central row by the function

$$P(z) = \prod_{j=j_0}^{j_1} \frac{(z-\rho_j)(z\tau_j - 1)}{ze^{-ik\eta_2\sin\psi_j}\,|e^{-ik\eta_2\sin\psi_j}|} \tag{10.1}$$

to remove the poles. This has the three symmetries that $d(z)$ inherits from the properties of the kernel matrix discussed in Section 6; thus

$$P(z) = \begin{cases} P^*(1/z^*) & \text{in all cases,} \\ P(1/z) & \text{if } \eta_1 = 0, \\ P\left(\dfrac{1}{ze^{ika_1\cos\psi_0}}\right) & \text{if } 2\eta_1 = a_1. \end{cases} \tag{10.2}$$

The factor $|e^{-ik\eta_2\sin\psi_j}|$ is included in the denominator to normalise the magnitude of $P(z)$. Since $P(z)d(z)$ is real and analytic on the unit circle, zeros here can be located using standard methods. In the case of a rectangular lattice, where $\eta_1 = 0$, it is often but not always the case that zeros not on the unit circle are located on the real line. In this case we can combine the two available symmetry relations to show that $P^*(z^*)d^*(z^*) = p(z)d(z)$, so that $z^{j_1-j_0+1}P(z)d(z)$ is real and analytic for $z \in \mathbb{R}$. Any roots that occur here can also be located fairly easily, though the search algorithm must take account of the fact that pairs

of roots sometimes appear very close to the origin. A similar situation occurs for lattices with $\eta_1 = a_1/2$, when the roots with $|z| \neq 1$ are often but not always located on the line $z = ue^{-ik\eta_1 \cos\psi_0}$, $u \in \mathbb{R}$, and here $u^{j_1-j_0+1}P(z)d(z)$ is real and analytic. For other cases, we observe that the residues of the determinant at its poles can be calculated using (7.11), and these can be used to express $d(z)$ as a sum of partial fractions. This can easily be differentiated, so that the Newton–Raphson method becomes available. Using the origin as the initial guess often yields one root, w_0^{-1}, say, and then a second can sometimes be obtained by applying the Newton–Raphson iteration to $d(z)/(z - w_0^{-1})$, again using the origin as the initial guess. Any roots not determined by these elementary methods can be calculated using the technique in (**30**). This is computationally expensive, and we do not claim that it is the optimal approach, but it is very reliable.

Once the zeros of the determinant have been calculated, the remaining computations are straightforward, and can be performed using standard libraries. First we classify any zeros that appear on the unit circle using (9.13). At each zero, we calculate the eigenvector of $\mathbf{L}(z)$ that corresponds to the zero eigenvalue. The elements of this eigenvector then play the role of B_n in (9.12), and the zero plays the role of z_0 in (9.14) and (9.15). We then determine the sign of the integral I_2 in (9.13). If $\mathrm{I}_2 > 0$, the zero corresponds to a Bloch wave that transports energy into the lattice. We denote this zero by z_p for an appropriate choice of the index p, and indent the contour Ω so that the point $z = z_p$ lies outside (see Fig. 2). On the other hand, if $\mathrm{I}_2 < 0$, the zero corresponds to Bloch wave that cannot be excited by a wave incident from below the lattice. Such zeros must lie inside the contour Ω and are denoted by w_p^{-1}. The residue coefficient b, which cannot be calculated at this stage, plays no part in this. Once the zeros are classified, we can calculate all of the eigenvectors $\mathbf{E}_p$ defined in (7.13), and the linear system (7.15) can be solved to obtain X_0^j. The functions $T_n^-(z)$ are then given explicitly by (7.8), and the problem is solved.

Next, we check that energy is conserved using (9.5). Whilst this is a necessary condition for the correctness of the results, it is by no means sufficient, and where methods involving modal expansions are used, it is sometimes possible to discard important terms and construct manifestly incorrect solutions that nonetheless conserve energy (**31**). A much more stringent test can be performed by calculating the coefficients A_n^p directly from (4.17) in cases where no Bloch waves are excited (so that $A_n^p \to 0$ as $p \to \infty$). We can also calculate A_n^p by collecting residues from outside the contour Ω in (5.8); equations (8.3)–(8.5) can be used at each pole. To test the results in cases where Bloch waves are excited, we use the infinite array subtraction technique introduced in (**32**). For a case with a single Bloch wave, (8.3) and (5.8) yield

$$A_n^p = -bB_n z_0^{-p-1} + \hat{A}_n^p, \tag{10.3}$$

where $\hat{A}_n^p \to 0$ as $p \to \infty$. We calculate b, B_n and z_0 as described above, and then use (10.3) in (4.17) to obtain

$$\hat{A}_n^q + Z_n \sum_{m=-\infty}^{\infty} \sum_{p=0}^{\infty} \hat{A}_m^p S_{m-n}^{q-p}(k\cos\psi_0) = -Z_n i^n e^{i(q\mathbf{a}_2\cdot\mathbf{k}-n\psi_0)} + \Delta_n^q, \quad n \in \mathbb{Z}, \quad q = 0, 1, \ldots \tag{10.4}$$

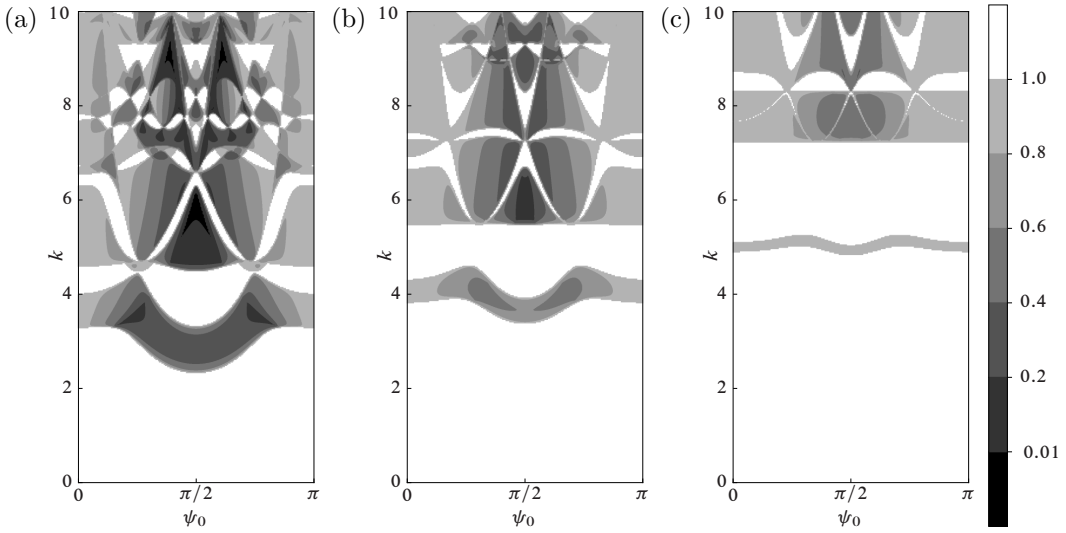

Fig. 4 Proportion of energy reflected back from a lattice with basis vectors $\mathbf{a}_1 = [1, 0]$ and $\mathbf{a}_2 = [0, 1]$. Dirichlet boundary conditions are enforced on the cylinder surfaces. (a) $\ell = 0.1$, (b) $\ell = 0.2$ and (c) $\ell = 0.3$.

where

$$\Delta_n^q = bz_0^{-q-1}\Bigg[B_n + Z_n \sum_{m=-\infty}^{\infty} B_m \sum_{p=0}^{\infty} e^{i(p-q)\mathbf{a}_2\cdot\boldsymbol{\beta}_0} S_{m-n}^{q-p}(k\cos\psi_0)\Bigg], \tag{10.5}$$

with $\boldsymbol{\beta}_0$ given by (8.10). Separating the terms with $p \le q$ from the remainder of the series, and using (4.11) and (A.5), this becomes

$$\Delta_n^q = bz_0^{-q-1}\Bigg[B_n + Z_n \sum_{m=-\infty}^{\infty} B_m \Big\{G_{m-n}^{(-q,-1)}(\mathbf{0}, \boldsymbol{\beta}_0) + \sigma_{n-m}(k\cos\psi_0) + e^{i\mathbf{a}_2\cdot\boldsymbol{\beta}_0} G_{m-n}^{(0,\infty)}(-\mathbf{a}_2, \boldsymbol{\beta}_0)\Big\}\Bigg]. \tag{10.6}$$

The multirow Green's functions that appear here can be calculated using (A.13) and (A.15); the first disappears in the case where $q = 0$. When (10.4) is solved by truncation, we find that $\hat{A}_n^p \to 0$ as $p \to \infty$, which means we can have confidence that the results are correct. To apply the same method to cases where multiple Bloch waves are excited, we need only include extra residue terms on the right-hand side of (10.3), evaluate (10.6) for each Bloch wave and include the results on the right-hand side of (10.4).

All of the results in the following section were generated using an implementation of our method written in Fortran 2003, using double precision arithmetic. The multipole truncation parameter N is set according to the value of $k\ell$; our implementation uses values chosen so that

$$|W_N| < 10^{-12} \max_{n \le N} |W_n|. \tag{10.7}$$

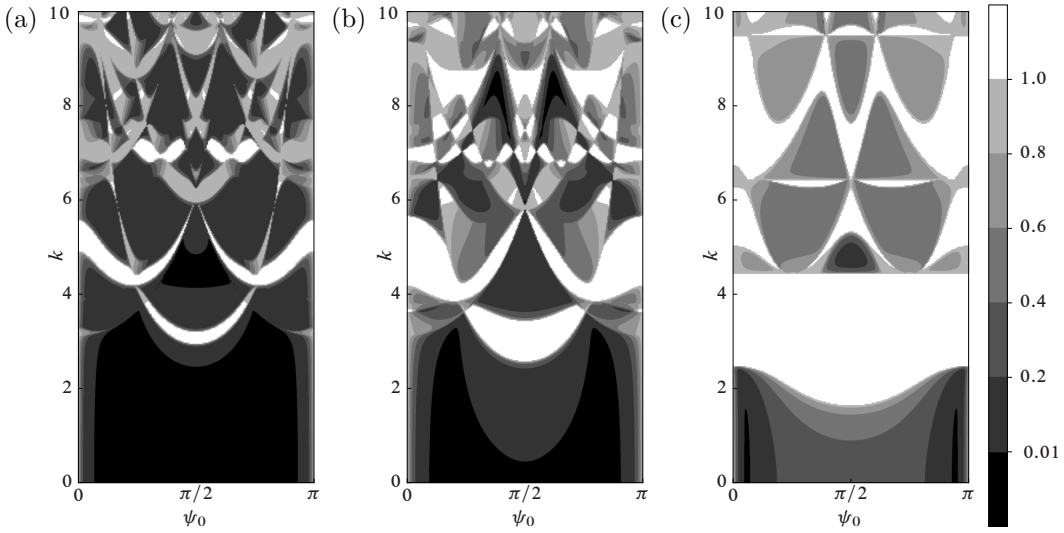

Fig. 5 Proportion of energy reflected back from a lattice with basis vectors $\mathbf{a}_1 = [1, 0]$ and $\mathbf{a}_2 = [0, 1]$. Neumann boundary conditions are enforced on the cylinder surfaces. (a) $\ell = 0.1$, (b) $\ell = 0.2$ and (c) $\ell = 0.45$.

Typically, increasing $k\ell$ increases the number of terms that must be retained in the multipole expansion. For example, for Dirichlet conditions, $N = 7$ is sufficient to satisfy (10.7) if $k\ell = 1$, whereas $N = 13$ is required if $k\ell = 4.5$. For the grating mode expansion, we discard terms for which

$$|e^{ik\eta_2 \sin\psi_j}| < \varepsilon^{\alpha}, \tag{10.8}$$

where ε represents machine epsilon (approximately 10^{-16} for double precision). The positive parameter α is chosen experimentally. Too small a value leads to modes that generate significant interactions between the rows being discarded, but too large a value leads to situations where the determinant possesses roots with very small magnitudes, which can cause numerical problems. We have found $\alpha \approx 0.35$ to be a good compromise choice.

11. Numerical results

The problem of Bloch wave propagation through lattices of sound-hard and sound-soft cylinders was investigated in (**33**). Here, we focus our attention on the proportions of incident wave energy that are reflected back from and transmitted into the lattice. To this end, we rewrite (9.5) in the form

$$E_T + E_R = 1, \tag{11.1}$$

where

$$E_T = \frac{2\mathrm{I}_2}{P_0 \omega k a_1 \sin\psi_0} \quad \text{and} \quad E_R = \frac{1}{\sin\psi_0} \sum_{j \in \mathcal{M}'} \left| X_0^j \right|^2 \sin\psi_j. \tag{11.2}$$

In a stop band, no energy can be transmitted into the lattice, so $E_T = 0$ and $E_R = 1$. However, when Bloch waves are excited it is not possible to determine E_R or E_T from an

understanding of the wave-bearing properties of the lattice alone. Consequently the results shown here reveal information about the behaviour of the field in pass bands and partial stop bands that cannot be obtained from a standard band diagram.

Figs. 4 and 5 show contour plots of E_R for square lattices, with ℓ increasing from left to right. Here, and in Figs. 6 and 7, light and dark regions indicate strong reflection and strong transmission, respectively. Note that the total field always disappears in the grazing limits $\psi_0 \to 0$ and $\psi_0 \to \pi$ so that $E_T = 0$. This was shown to be the case for a single array in (**25**) and the same result clearly holds for a semi-infinite lattice. However, the transition is often very rapid, so that the effect is not visible in contour plots, though it has been verified by inspecting the actual data. As we should expect, larger scatterers tend to reflect more of the energy back from the lattice, and the stop bands generally widen as ℓ is increased. It is also evident that a lattice formed from sound-hard (Neumann) scatterers generally permits a greater proportion of energy to be transmitted than the equivalent sound-soft (Dirichlet) lattice. At low frequencies, the plots for sound-soft scatterers shown in Fig. 4 exhibit a total stop band, the extent of which increases with ℓ, as noted in (**33**). Above this, there is a narrow band in which some transmission is possible, and for still higher values of k there is a second stop band. This is partial for small scatterers, that is it prevents propagation in certain directions, but there is no frequency at which no directions are permitted. As ℓ is increased, this region widens, becoming a total stop band. Above the second stop band, the pattern of transmission and reflection is very complicated, with multiple partial stop bands and some small regions where high transmission occurs. For $\ell = 0.35$ or greater (not shown), the corresponding plots are almost entirely occupied by the first and second stop bands, so that very little transmission is possible within this frequency range. The plots for sound-hard scatterers shown in Fig. 5 are quite different, with no low frequency stop band and much more substantial regions of high transmission. Indeed, at low frequencies there is a region in which $E_R < 0.01$, so that more than 99% of the incident wave energy is transmitted into the lattice. This region contracts as ℓ is increased, but it persists even in Fig. 5(c), where $\ell = 0.45$. A partial stop band can be seen for $k \approx 3$, even for very small scatterers, and for larger radii this becomes a total stop band, as in Fig. 5(c). Above this stop band, the pattern is again very complicated, but with more regions of high transmission than the sound-soft case.

Fig. 6 shows contour plots of E_R for rectangular lattices, with $\eta_2 > a_1$. In general, stretching the lattice causes the pattern to fragment, so that the regions of high and low transmission are smaller and more numerous. In particular, narrow regions where transmission is possible gradually penetrate into the first stop band for sound-soft scatterers, and similarly, the region of high transmission observed at low frequencies for sound-hard bodies is interspersed with partial stop bands.

In contrast to η_2, varying η_1 has fairly limited effects on the transmission patterns. For lattices with $\eta_2 = \eta_1/2$, which retain symmetry across $\psi_0 = \pi/2$, the plots are qualitatively similar to those in Figs. 4, 5 and 6, and are not shown here. Instead, Fig. 7 shows three situations in which the lattice is skewed. The effect of breaking symmetry across $\psi_0 = \pi/2$ is more pronounced for small scatterers, and some distortion is evident in Fig. 7(a) and (b). For larger scatterers such as those in 7(c), the plots are much more symmetric and qualitatively similar to the corresponding versions for the square lattice. One quantitative difference between Figs. 4(c) and 7(c) is that the second pass band is detached in the latter case, so that a third total stop band has appeared.

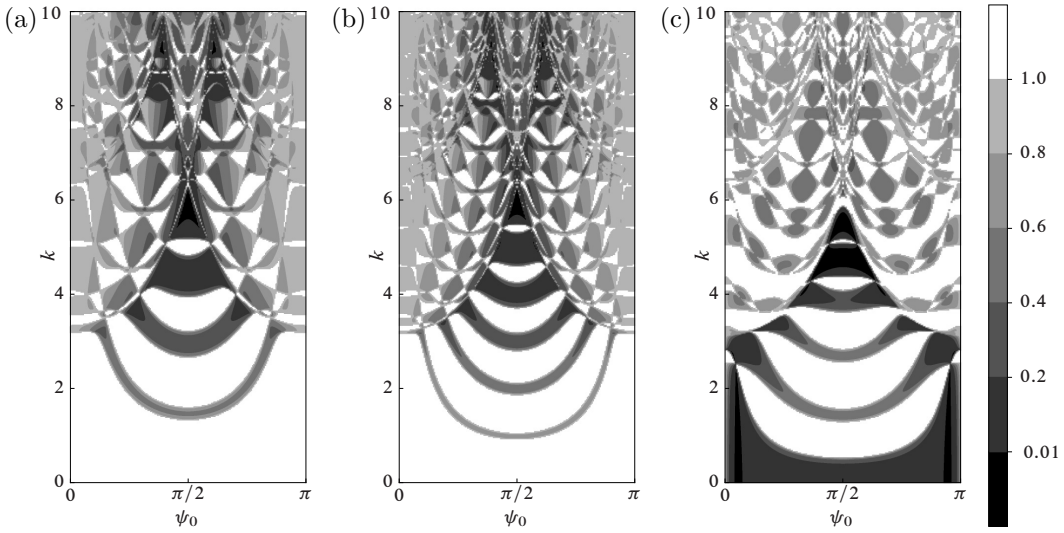

Fig. 6 Proportion of energy reflected back from lattices with $\mathbf{a}_1 = [1, 0]$, $\mathbf{a}_2 = [0, \eta_2]$ and $\eta_2 > a_1$. (a) Dirichlet boundary conditions, $\ell = 0.1$, $\eta_2 = 2$. (b) As (a) but with $\eta_2 = 3$. (c) Neumann boundary conditions, $\ell = 0.45$, $\eta_2 = 3$.

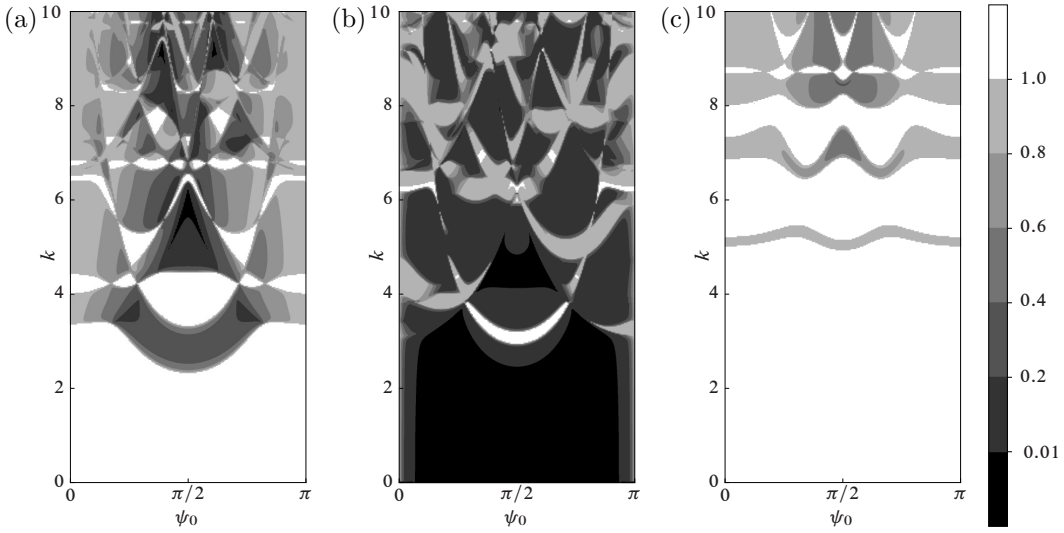

Fig. 7 Proportion of energy reflected back from a skewed lattice with $\mathbf{a}_1 = [1, 0]$ and $\mathbf{a}_2 = [0.25, 1.0]$. (a) Dirichlet boundary conditions, $\ell = 0.1$, (b) Neumann boundary conditions, $\ell = 0.1$, (c) Dirichlet boundary conditions, $\ell = 0.3$.

Finally, in Fig. 8, we present four plots of the field itself. The actual data shown are values of $\mathrm{Re}[u(\mathbf{r})]$, so that the plots show a snapshot of $U(\mathbf{r}, t)$ at time $t = 0$. At most points, the

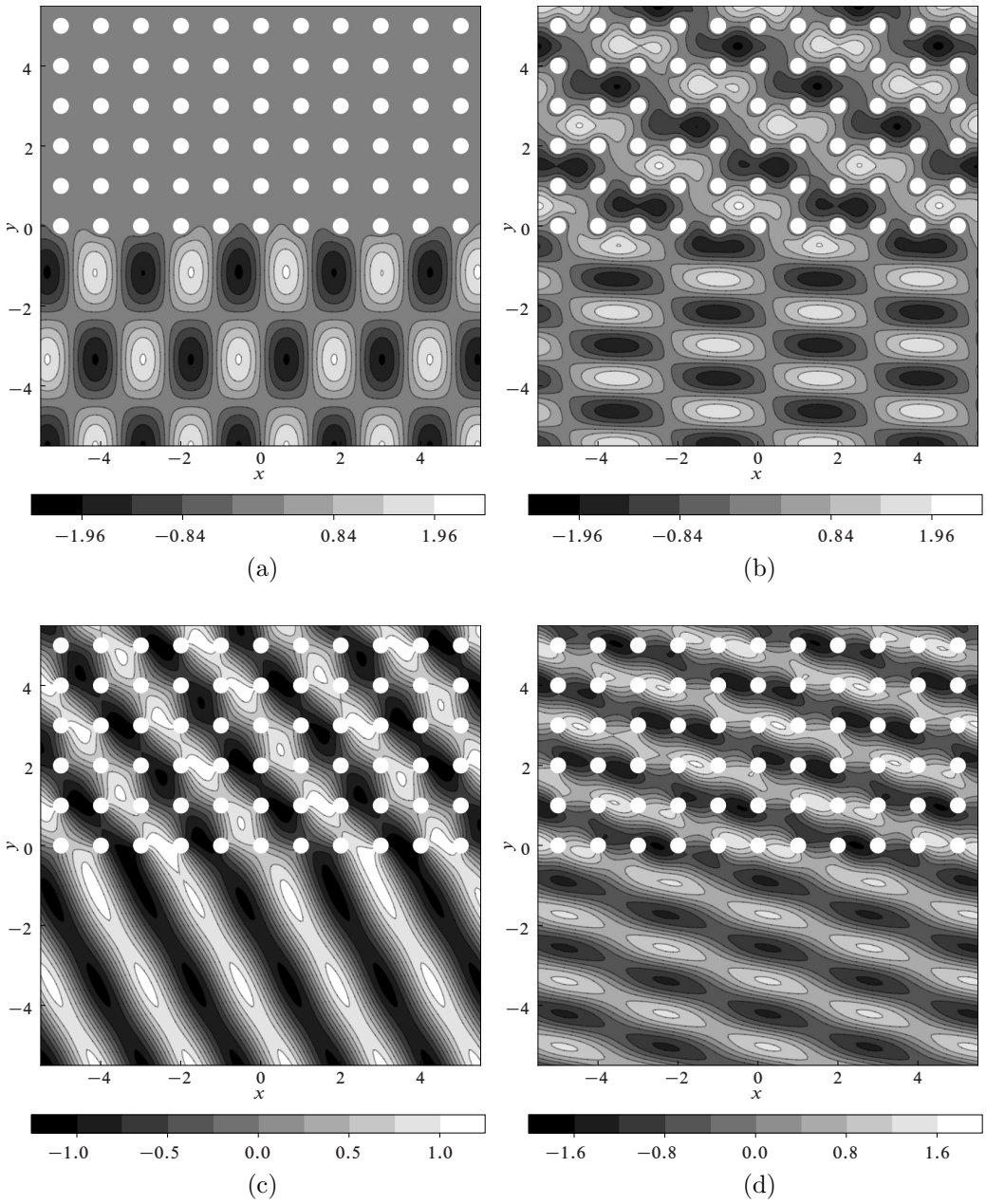

Fig. 8 Contours plot showing the real part of the field for a lattice with $\mathbf{a}_1 = [1, 0]$, $\mathbf{a}_2 = [0, 1]$ and $\ell = 0.2$. (a) Dirichlet boundary conditions, $k = 3.0$, $\psi_0 = 0.16\pi$. (b) Dirichlet boundary conditions, $k = 4.0$, $\psi_0 = 0.4\pi$. (c) As (a), but with Neumann conditions. (d) As (b), but with Neumann conditions.

field is evaluated using the quasi-periodic Green's functions in appendix A, but close to the cylinder centred at $\mathbf{r} = j\mathbf{a}_1 + p\mathbf{a}_2$, we use the fact that (**25**)

$$u(\mathbf{r}) = \sum_{n=-\infty}^{\infty} e^{ijka_1 \cos\psi_0} A_n^p \left[\mathcal{H}_n(\mathbf{r}) - \frac{1}{Z_n} \mathcal{J}_n(\mathbf{r}) \right]. \tag{11.3}$$

In Fig. 8(a) and (b), Dirichlet boundary conditions are imposed on the surface of the scatterers and it is evident that the field is close to zero in their immediate vicinity. Similarly, in Fig. 8(c) and (d) the contours intersect the scatterers at right angles, showing that the Neumann boundary conditions enforced on the surfaces are indeed satisfied. Bloch waves are excited in (b), (c) and (d), and the different nature of the field inside and outside the lattice is clearly visible. On the other hand, no Bloch waves are excited in (a); note that the decay of the field as y is increased from zero is extremely rapid. In Fig. 8(b) we have $E_R \approx 0.65$ whereas in (c) and (d) we have $E_R \approx 0.0071$, and $E_R \approx 0.075$, respectively (obviously $E_R = 1$ in (a)). Thus, (c) is an example of the near total transmission phenomenon predicted by Fig. 5(b), and in this case there is very little interference due to reflection below the lattice.

12. Concluding remarks

We have determined the field that arises when a time-harmonic plane wave impinges upon a semi-infinite lattice of circular cylinders, using a full linear theory which allows for a wide range of frequencies and scatterer sizes. A representation of the far field in terms of grating modes has been obtained, and formulae for the coefficients in this expansion have been calculated, both for the exterior region and for the far-field limit inside the lattice. For a given set of parameters (angle of incidence, wavenumber and lattice geometry), these formulae can be computed by a combination of complex root finding and straightforward linear algebra. The proportion of incident energy reflected back from, and transmitted through, the edge can also be calculated in this way.

We have then investigated the transmission and reflection properties of lattices composed of sound-hard and sound-soft cylinders. These results contain substantial information that cannot be deduced from the band structure of the corresponding infinite periodic lattice. In particular, for sound-hard cylinders, there exist parameter regimes within which almost all of the incident energy is converted into Bloch waves and transmitted into the lattice. We have confirmed the correctness of our results using conservation of energy (a necessary but not sufficient condition), and a more stringent test based on infinite array subtraction.

There are many possible avenues for further research using the method developed in this paper. Lattice elements with noncircular cross sections can be accounted for using T-matrices (**14**, Chapter 7). Another possibility is to consider penetrable cylinders, and in the acoustic case, this extension is straightforward (see Section 1). Perhaps the most important and challenging possibility is the extension to the electromagnetic case. Here, certain configurations, such as oblique incidence on dielectric cylinders (**34**), lead to coupling between the electric and magnetic fields and this in turn necessitates the use of more complicated multipole expansions. The excitation of electromagnetic Bloch waves is intended as the subject for a future paper.

Acknowledgements

This article is based in part on research undertaken by the authors at Loughborough University (**35**).

References

1. M. Sigalas and E. N. Economou. Band structure of elastic waves in two-dimensional systems. *Solid State Commun.*, 86(3):141–143, 1993.
2. A. B. Movchan, N. V. Movchan, and R. C. McPhedran. Bloch–Floquet bending waves in perforated thin plates. *Proc. Roy. Soc. Lond., A*, 463:2505–2518, 2007.
3. N. V. Movchan, R. C. McPhedran, and A. B. Movchan. Flexural waves in structured elastic plates: Mindlin versus bi-harmonic models. *Proc. Roy. Soc. Lond., A*, 467:869–880, 2011.
4. Z. Zhang and S. Satpathy. Electromagnetic wave propagation in periodic structures: Bloch wave solution of Maxwell's equations. *Phys. Rev. Lett.*, 65(21):2650–2653, 1990.
5. P. McIver. Approximations to wave propagation through doubly-periodic arrays of scatterers. *Waves in Random and Complex Media*, 17(4):439–453, 2007.
6. R. V. Craster, T. Antonakakis, M. Makwana, and S Guenneau. Dangers of using the edges of the Brillouin zone. *Phys. Rev. B*, 86:6 pages, 2012.
7. T. Antonakakis, R. V. Craster, and S. Guenneau. Asymptotics for metamaterials and photonic crystals. *Proc. Roy. Soc. Lond., A*, 469:20 pages, 2013.
8. P. Russell. Photonic crystal fibers. *Science*, 299:358–362, 2003.
9. A. Yariv and P. Yeh. *Photonics: Optical Electronics in Modern Communications*. The Oxford Series in Electrical and Computer Engineering. Oxford University Press, 2007.
10. J. D. Joannopoulos, S. G. Johnson, J. N. Winn, and R. D. Meade. *Photonic crystals. Molding the Flow of Light*. Princeton University Press, 2nd edition, 2008.
11. N. Tymis and I. Thompson. Low frequency scattering by a semi-infinite lattice of cylinders. *Q. J. Mech. Appl. Math.*, 64:171–195, 2011.
12. M. Albani and F. Capolino. Wave dynamics by a plane wave on a half-space metamaterial made of plasmonic nanospheres: a discrete Wiener–Hopf formulation. *J. Opt. Soc. Am., B*, 28:2174–2185, 2011.
13. P. A. Belov and C. R. Simovski. Boundary conditions for interfaces of electromagnetic crystals and the generalized Ewald–Oseen extinction principle. *Phys. Rev. B*, 73:14 pages, 2006.
14. P. A. Martin. *Multiple Scattering. Interaction of Time-Harmonic Waves with N Obstacles*. Cambridge University Press, 2006.
15. C. M. Linton and P. McIver. *Handbook of Mathematical Techniques for Wave/Structure Interactions*. Chapman & Hall/CRC, Boca Raton, 2001.
16. C. M. Linton and P. A. Martin. Multiple scattering by random configurations of circular cylinders: second-order corrections for the effective wavenumber. *J. Acoust. Soc. Am.*, 117:3413–3423, 2005.
17. C. M. Linton and P. A. Martin. Semi-infinite arrays of isotropic point scatterers. A unified approach. *SIAM J. Appl. Math.*, 64(3):1035–1056, 2004.
18. F. Capolino and M. Albani. Truncation effects in a semi-infinite periodic array of thin strips: A discrete Wiener-Hopf formulation. *Radio Science*, 44:RS2S91 (1–14), 2009.

19. E. I. Jury. *Theory and Application of the z-Transform Method*. Robert E. Krieger Publishing, New York, 1964.
20. B. Noble. *Methods Based on the Wiener–Hopf Technique*. Chelsea, 1988.
21. I. D. Abrahams. On the solution of Wiener-Hopf problems involving noncommutative matrix kernel decompositions. *SIAM J. Appl. Math.*, 57(2):541–567, 1997.
22. I. D. Abrahams. On the non-commutative factorization of Wiener–Hopf kernels of Khrapkov type. *Proc. Roy. Soc. Lond., A*, 454:1719–1743, 1998.
23. F. W. J. Olver, D. W. Lozier, R. F. Boisvert, and C. W. Clark. *NIST Handbook of Mathematical Functions*. Cambridge University Press, 2010.
24. I. Thompson and C. M. Linton. Guided surface waves on one- and two-dimensional arrays of spheres. *SIAM J. Appl. Math.*, 70:2975–2995, 2010.
25. C. M. Linton and I. Thompson. Resonant effects in scattering by periodic arrays. *Wave Motion*, 44:167–175, 2007.
26. L. C. Botten, N. A. Nicorovici, R. C. McPhedran, C. Martijn de Sterke, and A. A. Asatryan. Photonic band structure calculations using scattering matrices. *Phys. Rev. E*, 64(4):046603 (18 pages), 2007.
27. M. A. Peter and Meylan M. H. Water-wave scattering by vast fields of bodies. *SIAM J. Appl. Math.*, 70:1567–1586, 2009.
28. I. Thompson and C. M. Linton. On the excitation of a closely spaced array by a line source. *IMA J. Appl. Math.*, 72(4):476–497, 2007.
29. Ivar Stakgold. *Green's Functions and Boundary Value Problems*. Wiley, 2nd edition, 1998.
30. B. Davies. Locating the zeros of an analytic function. *J. Comput. Phys.*, 18:36–49, 1986.
31. D. P. Warren, J. B. Lawrie, and I. M. Mohamed. Acoustic scattering in waveguides that are discontinuous in geometry and material property. *Wave Motion*, 36:119–142, 2002.
32. C. M. Linton, R. Porter, and I. Thompson. Scattering by a semi-infinite periodic array and the excitation of surface waves. *SIAM J. Appl. Math.*, 67(5):1233–1258, 2007.
33. N. A. Nicorovici, R. C. McPhedran, and L. C. Botten. Photonic band gaps for arrays of perfectly conducting cylinders. *Phys. Rev. E*, 52(1):1135–1145, 1995.
34. Ö. Kavaklioğlu. On Schlömilch series representation for the transverse electric multiple scattering by an infinite grating of insulating dielectric circular cylinders at oblique incidence. *J. Phys. A*, 35:2229–2248, 2002.
35. Nikolaos Tymis. *Analytical Techniques for Acoustic Scattering by Arrays of Cylinders*. PhD thesis, Loughborough University, 2012.
36. C. M. Linton. Lattice sums for the Helmholtz equation. *SIAM Review*, 52:630–674, 2010.

APPENDIX A

Green's functions for one- and two-dimensional arrays

In this appendix, we obtain spectral forms for the one- and two-dimensional quasi-periodic Green's functions

$$G_n(\mathbf{r}, \beta_x) = \sum_{j=-\infty}^{\infty} e^{ija_1\beta_x} \mathcal{H}_n(\mathbf{r} - \mathbf{R}_j), \tag{A.1}$$

and

$$G_n^{(q_0,q_1)}(\mathbf{r},\boldsymbol{\beta}) = \sum_{q=q_0}^{q_1}\sum_{j=-\infty}^{\infty} e^{i\mathbf{R}_{jq}\cdot\boldsymbol{\beta}}\mathcal{H}_n(\mathbf{r}-\mathbf{R}_{jq}), \tag{A.2}$$

where the vectors $\mathbf{R}_j$ and $\mathbf{R}_{jq}$ are given by

$$\mathbf{R}_j = j\mathbf{a}_1 = ja_1\hat{\mathbf{x}}, \tag{A.3}$$

and

$$\mathbf{R}_{jq} = j\mathbf{a}_1 + q\mathbf{a}_2 = (ja_1 + q\eta_1)\hat{\mathbf{x}} + q\eta_2\hat{\mathbf{y}}, \tag{A.4}$$

respectively. Note that (A.2) is related to (A.1) via

$$G_n^{(q_0,q_1)}(\mathbf{r},\boldsymbol{\beta}) = \sum_{q=q_0}^{q_1} e^{iq\mathbf{a}_2\cdot\boldsymbol{\beta}} G_n(\mathbf{r}-q\mathbf{a}_2,\beta_x), \tag{A.5}$$

where we have written $\boldsymbol{\beta} = \beta_x\hat{\mathbf{x}} + \beta_y\hat{\mathbf{y}}$. For the case where $n = 0$, (A.1) and (A.2) are quasi-periodic Green's functions in the 'classical' sense (phase shifted arrays of sources), and the results we require are given in (**11**). To allow n to take any integer value, we use the method from (**14**, ch. 2), and introduce the operator

$$\mathcal{D} \equiv -\frac{1}{k}\left(\frac{\partial}{\partial x} + i\frac{\partial}{\partial y}\right). \tag{A.6}$$

By converting $\mathcal{D}$ into polar coordinates, (**14**, Theorem 2.7) shows that repeated application yields

$$\mathcal{D}^n\mathcal{H}_0(\mathbf{r}) = \mathcal{H}_n(\mathbf{r}), \quad n > 0. \tag{A.7}$$

and

$$[-\mathcal{D}^*]^{-n}\mathcal{H}_0(\mathbf{r}) = \mathcal{H}_n(\mathbf{r}), \quad n < 0. \tag{A.8}$$

Therefore we may proceed by applying $\mathcal{D}$ and $-\mathcal{D}^*$ to the results in (**11**). For (A.1), we use (**11**, Equation (A7)) and we find that

$$G_n(\mathbf{r},\beta_x) = 2(-i)^{n+1}\sum_{j=-\infty}^{\infty}\frac{e^{ix\beta_{xj}-\gamma(\beta_{xj})|y|}}{a_1\gamma(\beta_{xj})}\left[\frac{k}{\beta_{xj}+\gamma(\beta_{xj})}\right]^{n\,\mathrm{sgn}(y)}, \tag{A.9}$$

where the function γ is given by (3.3),

$$\beta_{xj} = \beta_x + 2j\pi/a_1, \tag{A.10}$$

and we have made use of the identity

$$\frac{z-\gamma(z)}{k} = \frac{k}{z+\gamma(z)}. \tag{A.11}$$

If $\beta_x = k\cos\psi_0$, then we introduce the scattering angles using (3.2), and (A.9) becomes

$$G_n(\mathbf{r},k\cos\psi_0) = \frac{2(-i)^n}{ka_1}\sum_{j=-\infty}^{\infty}\frac{e^{in\,\mathrm{sgn}(y)\psi_j}}{\sin\psi_j}e^{ik(x\cos\psi_j+|y|\sin\psi_j)}. \tag{A.12}$$

For (A.2), we consider cases where $y - q\eta_2$ is of fixed sign for $q = q_0,\ldots,q_1$ (i.e. the observer is located above or below the entire array). We can use a linear combination of these to evaluate a quasi-periodic Green's function for an observer located between two rows, but note that these

spectral representations are not valid if the observer is located on the axis of a row, unless $n = 0$. Applying $\mathcal{D}$ and $-\mathcal{D}^*$ to (**11**, Equation (B5)), we obtain

$$G_n^{(q_0,q_1)}(\mathbf{r},\boldsymbol{\beta}) = 2(-i)^{n+1} \sum_{j=-\infty}^{\infty} \frac{e^{i\beta_{xj}x \mp \gamma(\beta_{xj})y}}{a_1\gamma(\beta_{xj})} \left[\frac{k}{\beta_{xj} \pm \gamma(\beta_{xj})}\right]^n \frac{e^{q_0 w_j^{\pm}} - e^{(1+q_1)w_j^{\pm}}}{1 - e^{w_j^{\pm}}}, \quad \text{(A.13)}$$

where β_{xj} is given by (A.10), and we have written

$$w_j^{\pm} = \pm\eta_2\gamma(\beta_{xj}) + i(\eta_2\beta_y - 2j\pi\eta_1/a_1). \quad \text{(A.14)}$$

The upper and lower signs are to be taken when $y > q_1\eta_2$ and $y < q_0\eta_2$, respectively. For semi-infinite arrays, (**11**, eqns. (B7) and (B8)) yield

$$G_n^{(0,\infty)}(\mathbf{r},\boldsymbol{\beta}) = 2(-i)^{n+1} \sum_{j=-\infty}^{\infty} \frac{e^{i\beta_{xj}x + \gamma(\beta_{xj})y}}{a_1\gamma(\beta_{xj})(1 - e^{w_j^-})} \left[\frac{k}{\beta_{xj} - \gamma(\beta_{xj})}\right]^n, \quad y < 0 \quad \text{(A.15)}$$

and

$$G_n^{(-\infty,-1)}(\mathbf{r},\boldsymbol{\beta}) = 2(-i)^{n+1} \sum_{j=-\infty}^{\infty} \frac{e^{i\beta_{xj}x - \gamma(\beta_{xj})y}}{a_1\gamma(\beta_{xj})(e^{w_j^+} - 1)} \left[\frac{k}{\beta_{xj} + \gamma(\beta_{xj})}\right]^n, \quad y > -\eta_2. \quad \text{(A.16)}$$

For $0 > y > -\eta_2$, the Green's function for the infinite lattice is obtained by adding the last two results. Equation (A.2) shows that this has the two-dimensional quasi-periodicity property

$$G_n^{(-\infty,\infty)}(\mathbf{r} + \mathbf{R}_{jq},\boldsymbol{\beta}) = e^{i\mathbf{R}_{jq}\cdot\boldsymbol{\beta}} G_n^{(-\infty,\infty)}(\mathbf{r},\boldsymbol{\beta}), \quad \text{(A.17)}$$

which facilitates evaluation between any consecutive pair of rows. Finally, if $\boldsymbol{\beta} = \boldsymbol{\beta}_0$ (8.10), then

$$\exp[w_j^+] = \frac{p_j}{z_0} \quad \text{and} \quad \exp[w_j^-] = \frac{1}{\tau_j z_0}, \quad \text{(A.18)}$$

meaning that

$$G_n^{(0,\infty)}(\mathbf{r},\boldsymbol{\beta}_0) = -2z_0(-i)^n \sum_{j=-\infty}^{\infty} \frac{e^{-in\psi_j} e^{ik(x\cos\psi_j - y\sin\psi_j)}}{ka_1\sin\psi_j(\tau_j^{-1} - z_0)}, \quad y < 0, \quad \text{(A.19)}$$

and

$$G_n^{(-\infty,-1)}(\mathbf{r},\boldsymbol{\beta}_0) = 2z_0(-i)^n \sum_{j=-\infty}^{\infty} \frac{e^{in\psi_j} e^{ik(x\cos\psi_j + y\sin\psi_j)}}{ka_1\sin\psi_j(\rho_j - z_0)}, \quad y > -\eta_2, \quad \text{(A.20)}$$

where ρ_j and τ_j are given by (5.15).

APPENDIX B

Lattice sums

The one-dimensional lattice sum σ_n, often called a Schlömilch series, is defined as

$$\sigma_n(\beta_x) = \sum_{\substack{j=-\infty \\ j\neq 0}}^{\infty} e^{ija_1\beta_x} \mathcal{H}_n(j\mathbf{a}_1). \quad \text{(B.1)}$$

Note that

$$\sigma_n(-\beta_x) = \sigma_{-n}(\beta_x) = (-1)^n\sigma_n(\beta_x). \quad \text{(B.2)}$$

Schlömilch series are related to the quasi-periodic Green's functions defined in (A.1) via the limit

$$\sigma_n^{(1)}(\beta_x) = \lim_{r\to 0}\big[G_n(\mathbf{r}, -\beta_x) - \mathcal{H}_n(\mathbf{r})\big]. \tag{B.3}$$

A number of formulae suitable for computing lattice sums are given in (**36**). In particular, if $\beta_x = k\cos\psi_0$, then

$$\sigma_0(\beta_x) = -1 - \frac{2i}{\pi}\Big(C + \ln\frac{ka_1}{4\pi}\Big) + \frac{2}{ka_1\sin\psi_0} + \sum_{\substack{j=-\infty\\ j\neq 0}}^{\infty}\Big(\frac{2}{ka_1\sin\psi_j} + \frac{i}{\pi|j|}\Big) \tag{B.4}$$

and

$$\sigma_n(\beta_x) = i^n\bigg[i\mathcal{B}_n(\beta_x) + \frac{2}{ka_1}\sum_{j=-\infty}^{\infty}\frac{e^{in\,\mathrm{sgn}(j)\psi_j}}{\sin\psi_j}\bigg], \quad n > 0, \tag{B.5}$$

where the scattering angles are defined in (3.2), $C \approx 0.5772$ is Euler's constant and we take $\mathrm{sgn}(0) = 1$. The function $\mathcal{B}_n$ is defined as

$$\mathcal{B}_n(\beta_x) = \frac{2}{n\pi}\cos\frac{n\pi}{2} + \frac{1}{\pi}\sum_{m=0}^{[(n-1)/2]}(-1)^m\frac{(n-m-1)!}{m!(n-2m)!}\Big(\frac{4\pi}{ka_1}\Big)^{n-2m}B_{n-2m}\Big(\frac{a_1\beta_x}{2\pi}\Big), \tag{B.6}$$

where $B_n(\cdot)$ represents a Bernoulli polynomial, and $[x]$ denotes the largest integer not greater than x. Schlömilch series with negative orders may be computed using the above formulae with (B.2).

APPENDIX C

Pathological cases

In Section 7, it was shown that the determinant $d(z)$ defined by (7.9) has at most simple poles at the points $z = \rho_j$ and $z = \tau_j^{-1}$, and no other singularities. In general, it has the form

$$d(z) = \mathsf{K}\prod_{j=j_0}^{j_1}\frac{(z - z_j)(w_j z - 1)}{(z - \rho_j)(\tau_j z - 1)}, \tag{C.1}$$

where K is a constant. For every set of parameters we have considered, the zeros w_j^{-1} are distinct from each other, and do not coincide with the poles. In this case, applying the Fredholm alternative to the approximate Wiener–Hopf equation (7.1) at each point $z = w_j^{-1}$ is sufficient to determine the coefficients X_0^j. Here we will show how our analysis can be modified to take other circumstances into account.

C.1 *$d(z)$ is the zero function*

If the rows of the matrix $\mathbf{K}(z)$ were to exhibit identical linear dependence (that is linear dependence for arbitrary z as opposed to at isolated points) then $d(z) \equiv 0$. Were this case to arise, the Fredholm alternative would also be satisfied at all points, and a sufficient number of equations to determine X_0^j could be obtained by choosing points arbitrarily.

C.2 *A zero coincides with a pole*

If $w_p = \tau_p$, then the number of zeros of the determinant is reduced by one, and the so the number of equations produced by the Fredholm alternative will be one lower than the number of unknowns. However, from (7.8), we have

$$T_n^-(z) - \frac{W_n}{W_0} i^n e^{in\psi_p} T_0^-(z) = i^n \sum_{j=j_0}^{j_1} X_o^j \left(\frac{e^{in\psi_j} - e^{in\psi_p}}{z\tau_j - 1} \right), \quad n \neq 0, \tag{C.2}$$

meaning that the row operations which produced the regularised kernel matrix $\mathbf{L}(z)$ in (7.11) also remove a pole from all but one of the rows in the right-hand side of (7.1). Therefore we form the matrix $\mathbf{M}$ by starting with the identity, and replacing the entries in the central column with

$$M_{n0} = \begin{cases} (w_p z - 1) & \text{if } n = 0, \\ -(W_n/W_0) i^n e^{in\psi_p} & \text{otherwise.} \end{cases} \tag{C.3}$$

Left-multiplying (7.1) by $\mathbf{M}$ removes the pole at $z = \tau_p^{-1}$ and restores the root of the determinant, so that the Fredholm alternative can be applied at this point.

C.3 *Higher order zeros*

Suppose that w_p^{-1} is a double root, and that all other roots of $d(z)$ are simple. Such a root may have two associated linearly independent eigenvectors, and in this case our method can be applied in the usual way. However, if only there is only one associated eigenvector, $\mathbf{E}_p$, the number of equations produced by the Fredholm alternative will again be one lower than the number of unknowns. We can obtain an extra equation as follows. Let r be chosen so that the entry in row r of the vector $\mathbf{E}_p$ is nonzero. Form the matrix $\mathbf{P}$ by starting with the identity, and replacing row r with $\mathbf{E}_p^*/(z - w_p^{-1})$. Since w_p^{-1} is a double root of $d(z)$, it follows that

$$\det\bigl[\mathbf{P}\mathbf{K}(w_p^{-1})\bigr] = 0. \tag{C.4}$$

Therefore we may left-multiply (7.1) by $\mathbf{P}$ and apply the Fredholm alternative again, provided we are able to take the limit $z \to w_p^{-1}$ in the central row. Here, we obtain

$$\frac{\mathbf{E}_p^*\mathbf{K}(z)}{z - w_p^{-1}} \mathbf{A}^+(z) = \frac{\mathbf{E}_p^*\mathbf{T}(z)}{z - w_p^{-1}}, \tag{C.5}$$

and, in view of (7.13) and (7.14), both ratios remain bounded in the limit $z \to w_p^{-1}$. Applying L'Hôpital's rule, we find that

$$\mathbf{E}_p^*\mathbf{K}'(w_p^{-1})\,\mathbf{A}^+(w_p^{-1}) = \mathbf{E}_p^*\mathbf{T}'(w_p^{-1}), \tag{C.6}$$

where the prime denotes differentiation of individual elements with respect to z. Other combinations of multiplicities can be dealt with in the same way, though the process becomes increasingly complicated for triple and higher order roots.